' Copy
RM L9H05

NACA

RESEARCH MEMORANDUM

CONTROL EFFECTIVENESS LOAD AND HINGE-MOMENT

CHARACTERISTICS OF A TIP CONTROL SURFACE

ON A DELTA WING AT A MACH NUMBER OF 1.9

By D. William Conner and Ellery B. May, Jr.

Langley Aeronautical Laboratory
Langley Air Force Base, Va.

NATIONAL ADVISORY COMMITTEE
FOR AERONAUTICS
WASHINGTON
October 7, 1949

NATIONAL ADVISORY COMMITTEE FOR AERONAUTICS

RESEARCH MEMORANDUM

CONTROL EFFECTIVENESS LOAD AND HINGE-MOMENT

CHARACTERISTICS OF A TIP CONTROL SURFACE
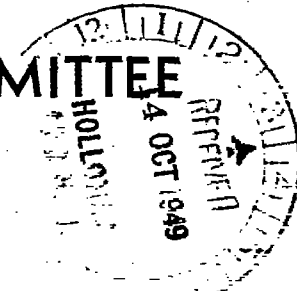
ON A DELTA WING AT A MACH NUMBER OF 1.9

By D. William Conner and Ellery B. May, Jr.

SUMMARY

A wind-tunnel investigation was made of a semispan delta wing
having the leading-edge swept back 60°. A half-delta control surface,
which made up the outer one-third of the exposed wing span, was hinged
about an axis perpendicular to the streamwise parting line separating
the control. Tests were made with and without a fence attached to the
inner wing panel at the parting line. Two controls were tested which
differed only in airfoil section. In addition to determining the charac-
teristics of the complete configuration, loads were measured on the con-
trol surface alone. The test Reynolds number was 4×10^6 and the free-
stream Mach number was 1.9.

The experimental rolling effectiveness of the control surface
amounted to about 85 percent of that calculated by linearized theory.
At zero angle of attack of the wing, the normal-force and moment charac-
teristics of the control were reasonably well predicted by linearized
theory. At low angles of attack, the control-surface hinge moment
exhibited considerable nonlinear variations with control deflection and
with angle of attack. Installation of the fence caused no significant
changes in the aerodynamic characteristics of the model. Increasing the
leading-edge bluntness of the control surface decreased the rolling
effectiveness and caused no change in the hinge-moment characteristics.

INTRODUCTION

Control surfaces which extend to the wing leading edge have been
found to be highly effective from subsonic speeds to moderate supersonic
speeds. (See reference 1.) Such types of full-chord controls appear to
have none of the reversals in effectiveness at transonic speeds which
characterize some trailing-edge flaps, probably because the effectiveness

is not unduly sensitive to flow separation near the wing trailing edge.
To learn more about such controls, an investigation has been conducted
in the Langley 9- by 12-inch supersonic blowdown tunnel on a half-delta
control mounted at the tip of a delta wing for a Mach number of 1.9 and
a Reynolds number of 4×10^6. Similar investigations are being under-
taken by the free-flight rocket technique, and acknowledgement is made
of rocket test data contained herein supplied by the Langley Pilotless
Aircraft Research Division.

The wing-model leading edge was swept back 60°, and the outer one-
third of the exposed span consisted of a tip control which rotated about
an axis normal to the root chord. In an attempt to minimize possible
gap effects caused by deflecting the control surface, tests were made
with a fence mounted at the outer end of the wing panel. Control sur-
faces of two thicknesses were tested. In some instances the results
have been compared with calculated characteristics.

COEFFICIENTS AND SYMBOLS

C_L lift coefficient $\left(\dfrac{Lift}{qS}\right)$

C_D drag coefficient $\left(\dfrac{Drag}{qS}\right)$

C_m pitching-moment coefficient $\left(\dfrac{M'}{qS\bar{c}}\right)$

C_l rolling-moment coefficient $\left(\dfrac{L}{2qSb}\right)$

C_n yawing-moment coefficient $\left(\dfrac{N}{2qSb}\right)$

M' pitching moment about center of area of
exposed wing

L rolling moment about axis of fuselage

N yawing moment about an axis perpendicular to
fuselage center line

$C_{N_f} = \dfrac{N_f}{qS_f}$

$$C_{C_f} = \frac{C_f}{qS_f}$$

$$C_{M_f} = \frac{M_f}{qS_f\bar{c}_f}$$

$$C_{BM_f} = \frac{BM_f}{qS_f b_f}$$

N_f control-surface force normal to control surface chord plane

C_f control-surface force chordwise along control surface chord plane

M_f control-surface pitching moment (hinge moment) about control-surface pivot axis

BM_f bending moment about root chord of control surface

$\dfrac{pb}{2V}\Big/\delta$ wing-tip helix angle in radians per degree control deflection $\left(\dfrac{C_{l_\delta}}{C_{l_p}}\right)$

C_{l_p} coefficient of damping in roll

q free-stream dynamic pressure

S exposed semispan wing area (19.94 sq in.)

S_f control-surface area (2.151 sq in.)

c local chord

$\bar{c}$ mean aerodynamic chord of exposed wing area (5.55 in.)

$\bar{c}_f$ mean aerodynamic chord of control surface (1.827 in.)

b twice distance from fuselage axis to wing tip (small fuselage, 11.17 in.; large fuselage, 12.37 in.)

b_f span of control surface from parting line to tip (1.570 in.)

t local thickness

α angle of attack measured with respect to free-stream direction

δ control-surface deflection measured with respect to wing chord plane in free-stream direction, degrees

R Reynolds number based on mean aerodynamic chord of exposed wing area

M Mach number

Subscripts:

α slope of curve of coefficient plotted against α

$$\left(\frac{dC_L}{d\alpha}, \frac{dC_l}{d\alpha}, \text{ and so forth} \right)$$

δ slope of curve of coefficient plotted against δ

$$\left(\frac{dC_L}{d\delta}, \frac{dC_l}{d\delta}, \text{ and so forth} \right)$$

MODEL

The system of axes is shown in figure 1. The semispan model of delta plan form had the leading edge swept back 60° and a corresponding aspect ratio of 2.3. A full-chord control surface was located at the wing tip. A photograph of the model mounted is shown as figure 2 and the principal dimensions are given in figure 3.

The main panel of the wing (inner two-thirds of the exposed span) was a flat plate, 3 percent thick at the fuselage intersection and 9 percent thick at the outboard end. The leading and trailing edges were beveled to wedge profiles with included wedge angles (parallel to

air stream) of 6.6° and 15.4°, respectively. The leading-edge wedge
was modified by a small nose radius, and the sharp breaks in contour
were modified by a slight fairing.

The control surface (outer one-third of the exposed span) was
separated from the inner panel of the wing by a streamwise parting line
and rotated about an axis perpendicular to the root chord. The axis
was located at 63 percent of the control-surface root chord. The basic
control was comprised of 3-percent-thick double-wedge airfoil sections
measured parallel to the air stream modified by a 0.9-percent-chord
leading-edge radius. A discontinuity in airfoil thickness existed at
the parting line between the control surface and main panel. Errors
in fabrication introduced a slight camber in the 3-percent-thick control
with a maximum displacement of the mean line near the point of maximum
thickness amounting to about 0.4 percent chord. An alternate control
surface was tested, identical in plan form to the basic surface but
having an airfoil section 7 percent thick with the maximum thickness far
forward.

Fences of two different sizes were tested on the main wing panel
at the parting line between the main wing panel and the control surface
(fig. 2(b)).

A few tests were made with a wing having no control surface but
having 9-percent-thick tip sections on the outer one-third of the
exposed wing span.

All tests of the wing and the control surface were made in the
presence of a half-fuselage. Fuselages of two different sizes were
used, both of which had the same nose shape. The nose section merged
into a constant-diameter section at the station where the wing leading
edge intersected the fuselage.

TUNNEL AND TEST TECHNIQUE

The Langley 9- by 12-inch supersonic blowdown tunnel, in which the
present tests were made, is a nonreturn tunnel utilizing the exhaust
air from the Langley 19-foot pressure tunnel. The inlet air enters at

an absolute pressure of about $2\frac{1}{3}$ atmospheres and contains about
0.3 percent of water by weight.

Semispan models are cantilevered from a 5-component strain-gage
balance mounted flush with the tunnel wall. The balance rotates with
the model as the angle of attack is changed and the forces and moments

are measured with respect to the balance axes. In measuring the forces
and moments acting on the control surface, the surface was connected
with the balance independent of the wing panel by means of a mounting
staff which extended spanwise through an internal slot in the main wing.
The half-span wing models are tested in the presence of, but not attached
to, a half-fuselage shimmed out 0.25 inch from the tunnel wall. The
finite gap existing between the wing and fuselage is believed to have no
influence on the flap loading. (See reference 2.)

The dynamic pressure and test Reynolds number decreased about 5 per-
cent during the course of each run because of the decreased pressure of
the inlet air. The average dynamic pressure was 11.8 pounds per square
inch, and the average Reynolds number, based on the mean aerodynamic
chord of the exposed wing, was 4.0×10^6.

PRECISION OF DATA

Free-stream Mach number has been calibrated at 1.90 ± 0.02. This
Mach number was used in determining the dynamic pressure. Calibration
tests which were made with the model removed indicated that the static
pressure varied about ±1.5 percent from a mean value for the region
normally occupied by the wing. A discussion is given in reference 2 of
the various factors which might influence the test results, such as
humidity effects and method of mounting.

An estimate has been made of the probable errors to be found in
the measured test points, when fluctuations in the readings of the
measuring equipment, calibration errors, and shift of instrument no-load
readings experienced during the course of each test are considered. The
following table lists the errors that might be expected to exist between
the test points for each particular figure.

Wing (figs. 4 to 9)		Control surface (initial series of tests) (figs. 13 and 14)		Control surface (second series of tests) (figs. 15 and 16)	
Variable	Error	Variable	Error	Variable	Error
α	$\pm 0.05^{\circ}$	α	$\pm 0.05^{\circ}$	α	$\pm 0.05^{\circ}$
δ	$\pm .2^{\circ}$	δ	$\pm .3^{\circ}$	δ	$\pm .2^{\circ}$
C_L	$\pm .003$	C_L	$\pm .001$	C_{N_f}	$\pm .005$
C_D	$\pm .001$	C_D	$\pm .001$	C_{C_f}	$\pm .010$
C_m	$\pm .001$	C_m	$\pm .001$	C_{M_f}	$\pm .008$
C_l	$\pm .0004$	C_l	$\pm .0002$	C_{BM_f}	$\pm .015$
C_n	$\pm .0003$	C_n	$\pm .0001$		

It should be noted that different geometric parameters and different axes were used in reducing the data for the two series of control-surface tests. The electrical system of the balance was arranged to permit direct moment measurements about the wing axes in the first series of tests and about the control axes in the second series. This technique was found necessary to avoid the introduction of considerable scatter in the moment data which appeared when an attempt was made to transfer the data to axes far distant from the point of measurement. From one model set-up to another (change in fence, fuselage, or control-surface thickness) the angle of attack could have differed by $\pm 0.1^{\circ}$, the control deflection could have differed by $\pm 0.4^{\circ}$, and the fuselage incidence with respect to the wing could have varied by $\pm 0.3^{\circ}$. Repeat tests were made for each configuration to assess the magnitude of errors. Static calibration indicated no measurable change in control-surface deflection caused by control-surface loading.

RESULTS

Figures 4 to 9 present test data of the complete wing as plots of the aerodynamic coefficients plotted against angle of attack for each of the various deflection angles of the tip control surface. Figure 10 presents cross plots of these data in which the coefficients are plotted against control deflection at zero angle of attack. Fuselage incidence is believed to have caused the displacement in the curves of figure 8 at zero deflection.

Figure 11 presents the variation of the rolling-effectiveness parameter $\frac{pb}{2V}\bigg/\delta$ with Mach number as obtained from free-flight rocket tests at two control deflections, wind-tunnel tests, and calculations based upon linearized theory. The rocket configuration (unpublished data) was tested by the Langley Pilotless Aircraft Research Division by the same technique and subject to the same limitations as the investigation of reference 1. The wing of rocket configuration had the large fence installed and operated at a Reynolds number of about 10×10^6 for the maximum Mach number of 1.5. In the region of the wing, the rocket fuselage diameter relative to the exposed wing span lay between the small fuselage and the large fuselage combinations of the wind-tunnel configurations. The fuselage nose of the rocket vehicle extended much farther ahead of the wing. The wind-tunnel test point was obtained from an average value of the experimental rolling effectiveness of the small fuselage configuration (reported herein) divided by an experimental damping coefficient C_{l_p} (from reference 3). To account for difference in fuselage diameters, the experimental rolling effectiveness was multiplied by a factor of 1.02, which is the theoretical ratio between the spanwise location in percent semispan of the control-surface loading for the rocket and the wind-tunnel configurations. The experimental damping coefficient included the effect of a fuselage (having about the same diameter relative to the wing span as did the present configuration) and had a value of 85 percent of that calculated for a flat-plate delta wing by linearized theory (reference 4). The calculations of $\frac{pb}{2V}$ by linearized theory utilized the method of reference 5 to obtain the rolling moment caused by control deflection and the method of reference 4 to obtain the damping coefficient (ignoring fuselage effects). Figure 12 presents the lift-drag curves of several configurations differing in tip thickness and in the fairing of the airfoil contours.

Figures 13 and 14 present the data first obtained for the control surface alone tested in the presence of the wing panel both with fence off and with large fence on. The coefficients in this figure are based on the wing dimensions and the moments are taken about the wing wind axes. Cross plots of these data at zero angle of attack are shown in figure 15 along with comparable data for the complete wing.

The second series of control-surface tests were made after first stiffening the balance structure (to increase the angle-of-attack range) and shifting the electrical center of the balance moment measuring components to the axes of the control surface. The data for these tests are presented in coefficient form (figs. 16 and 17) and include

normal force C_{N_f}, chord force C_{C_f}, pitching moment about the control

pivot axis C_{M_f}, and the bending moment about the root chord of the

control C_{BM_f}. Cross plots of these data are presented in figure 18 for

angles of attack of 0°, 2°, and 4°. Since the model had symmetrical
airfoil sections, all angles and coefficients can arbitrarily be reversed
in sign. This change in sign makes possible the application of the test
data to cover the condition of negative deflection angles for the
control. This procedure has been followed in presenting the cross-plot
data of figure 18 to show the nature of the curve shapes in the negative
range of control deflections. In going from negative to positive deflec-
tions, a discontinuity exists in most curves as a result of inaccuracies
in the test measurements.

DISCUSSION

Wing Characteristics

Control undeflected.- With the 3-percent-thick tip, the value of
the wing lift-curve slope C_{L_α} for both fuselage conditions was
about 0.040. The calculated value based on flat-plate theory (reference 6)
corrected by an estimate of the additional lift resulting from fuselage
upwash (reference 7) was 0.047 for the small fuselage and 0.049 for the
large fuselage. The minimum drag coefficient was about 0.012 with the
large fuselage and 0.013 with the small fuselage. Based on the lift
and pitching-moment data of figures 4 to 9, the chordwise location of
the aerodynamic center was 7 percent of the wing mean aerodynamic chord
ahead of the center of area. Similarly the lift and rolling-moment slopes
indicated the spanwise center of pressure to be located about 40 percent
of the exposed half-span outboard of the wing-fuselage juncture.

Control surface deflected.- Deflecting the control surface in the
positive direction tended to increase the value of minimum drag coeffi-
cient and to displace negatively the curves of pitching moment plotted
against angle of attack. The drag and yawing-moment curves were shifted
in the negative angle-of-attack direction since the wing drag load at
negative angles of attack tended to be counteracted by a decreased
control-deflection loading (control more alined with the air stream).

Within the accuracy of the test data, the various coefficients
varied linearly with control deflection at $\alpha = 0°$ (fig. 10). The
values of C_{L_δ} and C_{m_δ} were about 0.004 and -0.0013 as compared with

calculated values of 0.0045 and -0.0015, respectively. With regard to rolling moment, the curves of the three fence configurations (3-percent-thick control, fig. 10(a)), agreed within the experimental accuracy, and the average value of C_{l_δ} was 0.00076 for the small fuselage as compared

with a calculated value of 0.00090. This experimental value was used, as described in the section entitled "Results," to obtain a value

of $\frac{pb}{2V}\Big/\delta$ of 0.0058 radian per degree for $M = 1.9$ (fig. 11). The value

of $\frac{pb}{2V}\Big/\delta$, which is the ratio of C_{l_δ} to C_{l_p} (both based on the same

area and span), was in good agreement with theory. The agreement was somewhat fortuitous, however, since both experimental values $\left(C_{l_\delta}\text{ and }\right.$

$\left.C_{l_p}\right)$ were about 15 percent lower than the corresponding calculated

values. The data of figure 11 show agreement between the rocket test results and theory at supersonic speeds.

Effect of fence.- Adding a fence to the wing at the juncture of the wing panel and the control surface did not appreciably change the aerodynamic characteristics of the wing. There was no change in the drag characteristics or in the rolling effectiveness of the control (within the experimental accuracy), and the use of a fence of the dimensions investigated at this Mach number appears unwarranted.

Effect of airfoil-section modifications.- Increasing the control-surface thickness from 3 to 7 percent and moving the position of maximum thickness far forward increased the minimum drag coefficient less than 0.001 (fig. 12). Lift effectiveness of the control was decreased slightly and was accompanied by a 15-percent decrease in control rolling effectiveness.

When the airfoil sections comprising the outer one-third of the exposed wing panel were increased from 3- to 9-percent thickness (with the thickness distribution unchanged), the minimum drag coefficient was increased about 0.002 (fig. 12). In the initial configuration of the wing with 9-percent-thick tip sections, the wing airfoil sections were composed of flat-side elements with unfaired intersections. Rounding the nose of the airfoil increased the minimum drag, whereas incorporating fairing to eliminate sharp breaks in contour decreased the minimum drag. As the lift coefficient was increased, the differences in drag for the various configurations decreased. These results are for tests where the Mach line lies just ahead of the wing leading edge.

Control-Surface Characteristics

Division of loading between the control surface and the inboard panel of the wing.- A comparison of the slope values for the curves of figures 8 and 14 gives a measure of the part of the angle-of-attack loading carried on the control. The control surface covered 11 percent of the wing area and carried 18 percent of the lift load due to changing angle of attack C_{L_α}. High tip loading would be expected, because the highest loading on a sweptback wing is carried on the rays originating from the wing apex which lay in the region of the leading edge. The ratio of the value of C_{l_α} for the control surface to the value of C_{l_α} for the complete wing indicates that the lift load on the control surface was responsible for about one-fourth of the wing-panel rolling moment.

A part of the additional loading caused by control-surface deflection was carried on the inner panel of the wing (fig. 15), substantiating the carry-over loading indicated in reference 5. The experimental value of C_{L_δ} was 0.003 for the control surface and 0.004 for the complete wing. These values compare with calculated values of 0.0036 and 0.0045, respectively. The measured C_{l_δ} value of 0.00068 for the control surface was less than the previously mentioned value of 0.00078 for the complete wing with large fuselage.

Control-surface loading.- The results of the initial series of tests in which loads were measured on the control alone (figs. 13 to 15), though limited in scope, indicated that the fence had little effect on the loading of the control surface. The results of the second series of tests (figs. 16 to 18) permit a more detailed analysis of control-surface loading.

With the control surface undeflected, the value of $C_{N_{f_\alpha}}$ was about 0.065 (value calculated by linear theory was 0.078). As the control was deflected, $C_{N_{f_\alpha}}$ decreased in value especially at the highest deflections. The moment coefficient about the hinge line C_{M_f}, which corresponds to the control-surface hinge moment, varied nonlinearly with angle of attack as a result of a rearward shift in center of pressure which occurred when the wing was rotated from a streamwise direction. This effect was not defined at high control deflections since the angle-of-attack range did not include zero incidence.

The hinge-moment coefficient also varied nonlinearly with control deflection for high control deflections. (See fig. 18.) Increasing the angle of attack aggravated this condition at least in the well-defined range of negative deflections and appeared to decrease the linear

NACA RM L9H05

range of the moment curves. Both normal-force and bending-moment
coefficients varied almost linearly with control deflection for each
angle of attack, indicating that the change in hinge-moment characteris-
tics probably was associated with a change in load distribution near the
nose of the control root. Such a change in load distribution could well
be expected in this region because of the discontinuity in the chord
plane accompanying control deflection combined with a peak angle-of-
attack loading near the leading edge. Increasing the control-surface
thickness increased the chord-force coefficient. This increase, however,
would be of little practical significance from design considerations
since the maximum value of chord-force coefficient obtained was no
greater than 0.04 and was quite small when compared with normal-force
loads. The value of $C_{N_{f_\delta}}$ was decreased about 10 percent, and the

hinge-moment characteristics remained unchanged.

A comparison of theory with the experimental results for zero
angle of attack (fig. 18) indicates that flat-plate linearized theory
predicted reasonably well the variation of the coefficients with control
deflection though the theoretical normal-force effectiveness was not
fully realized.

CONCLUSIONS

From an investigation at a Mach number of 1.9 of a delta wing with
half-delta control flap in the Langley 9- by 12-inch supersonic blowdown
tunnel, the following conclusions may be drawn:

1. The experimental rolling effectiveness of the control amounted
to about 85 percent of that calculated by linearized theory.

2. At zero angle of attack of the wing, the normal-force, hinge-
moment, and bending-moment characteristics of the control surface were
in reasonable agreement with linearized theory. At small angles of
attack the control-surface hinge moment exhibited considerable nonlinear
variations with control deflection and with angle of attack.

3. Installation of the fence caused no significant changes in either
the aerodynamic characteristics of the complete wing or in the loads
and moments of the control surface.

4. Increasing the leading-edge bluntness and airfoil thickness of the control surface decreased the rolling effectiveness about 15 percent and caused no change in the hinge-moment characteristics.

Langley Aeronautical Laboratory
    National Advisory Committee for Aeronautics
        Langley Air Force Base, Va.

<div align="center">REFERENCES</div>

1. Sandahl, Carl A.: Free-Flight Investigation of the Rolling Effectiveness of Several Delta Wing-Aileron Configurations at Transonic and Supersonic Speeds. NACA RM L8D16, 1948.

2. Conner, D. William: Aerodynamic Characteristics of Two All-Movable Wings Tested in the Presence of a Fuselage at a Mach Number of 1.9. NACA RM L8H04, 1948.

3. Brown, Clinton E., and Heinke, Harry S., Jr.: Preliminary Wind-Tunnel Tests of Triangular and Rectangular Wings in Steady Roll at Mach Numbers of 1.62 and 1.92. NACA RM L8L30, 1948.

4. Brown, Clinton E., and Adams, Mac C.: Damping in Pitch and Roll of Triangular Wings at Supersonic Speeds. NACA Rep. 892, 1948.

5. Lagerstrom, P. A., and Graham, Martha E.: Linearized Theory of Supersonic Control Surfaces. Jour. Aero. Sci., vol. 16, no. 1, Jan. 1949, pp. 31-34.

6. Brown, Clinton E.: Theoretical Lift and Drag of Thin Triangular Wings at Supersonic Speeds. NACA Rep. 839, 1946.

7. Beskin, L.: Determination of Upwash around a Body of Revolution at Supersonic Velocities. CVAC-DEVF Memo BB-6, APL/JHU-CM-251, The Johns Hopkins Univ., Appl. Phys. Lab., May 27, 1946.
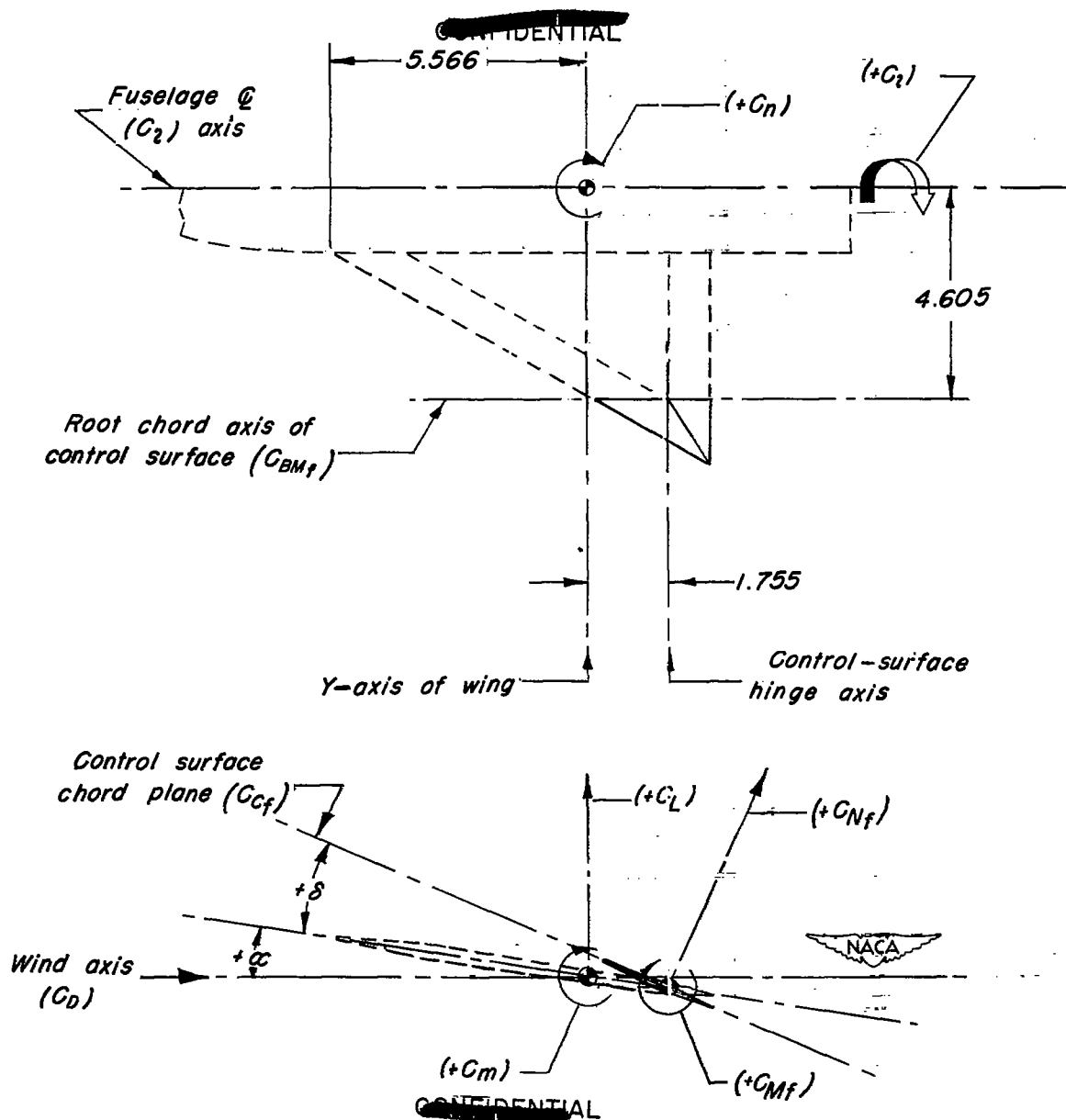
Figure 1.- Relation between the various reference axes and reference
   planes used in presenting test data for control surface. All
   dimensions in inches.

Figure 2.- Model mounted in the Langley 9- by 12-inch supersonic blowdown tunnel.

CONFIDENTIAL

5.60

8.326

0.80

¢

Fence

FUSELAGE ORDINATES

Large		Small	
Sta.	Rad.	Sta.	Rad.
0	.067	0	.038
.024	.073	.014	.042
.049	.084	.028	.048
.098	.089	.056	.051
.192	.117	.109	.067
.294	.140	.168	.080
.490	.185	.280	.150
.980	.292	.560	.167
1.920	.490	1.097	.285
2.940	.689	1.680	.394
3.920	.862	2.240	.493
4.900	1.001	2.800	.573
5.880	1.115	3.360	.636
6.860	1.202	3.920	.688
7.850	1.290	4.480	.735
8.830	1.354	5.050	.770
9.800	1.400	5.600	.800

0.024 radius normal
to leading edge

0.25 flat plate

15.4°

6.6°

Tip support beam

Section A—A
(enlarged)

0.075 radius

0.004 gap

0.008 gap

0.005 gap

A

A

4.785

60.1°

0.02 gap on each
side for zero load

5.585

6.185

0.25 inch micarta
shims

Station

Radius

5.60

12.20

9.80

Ref. planes

NACA

(a) Complete wing and fuselage; mean aerodynamic chord, 5.55; span (small fuselage), 11.17;
span (large fuselage), 12.37.

Figure 3.- Details of model. All dimensions are in inches.

0.376
2.740
0.241

1.735

Wing ℄

0.348

0.232

Tip center
rotation

Large fence
(0.009" thick)

0.024 l.e. radius at
root — tapers to
tip.

2.740
0.083

1.735

.03 t/c control

2.740

.190

.523

.07 t/c control

0.075 radius

1.570

60.2°

NACA

Pins soldered to
control to fix control
deflections.

Hinge line

0.174
2.740
0.116

1.735

Wing ℄

0.174

0.116

Tip center
rotation

Small fence
(0.009" thick)
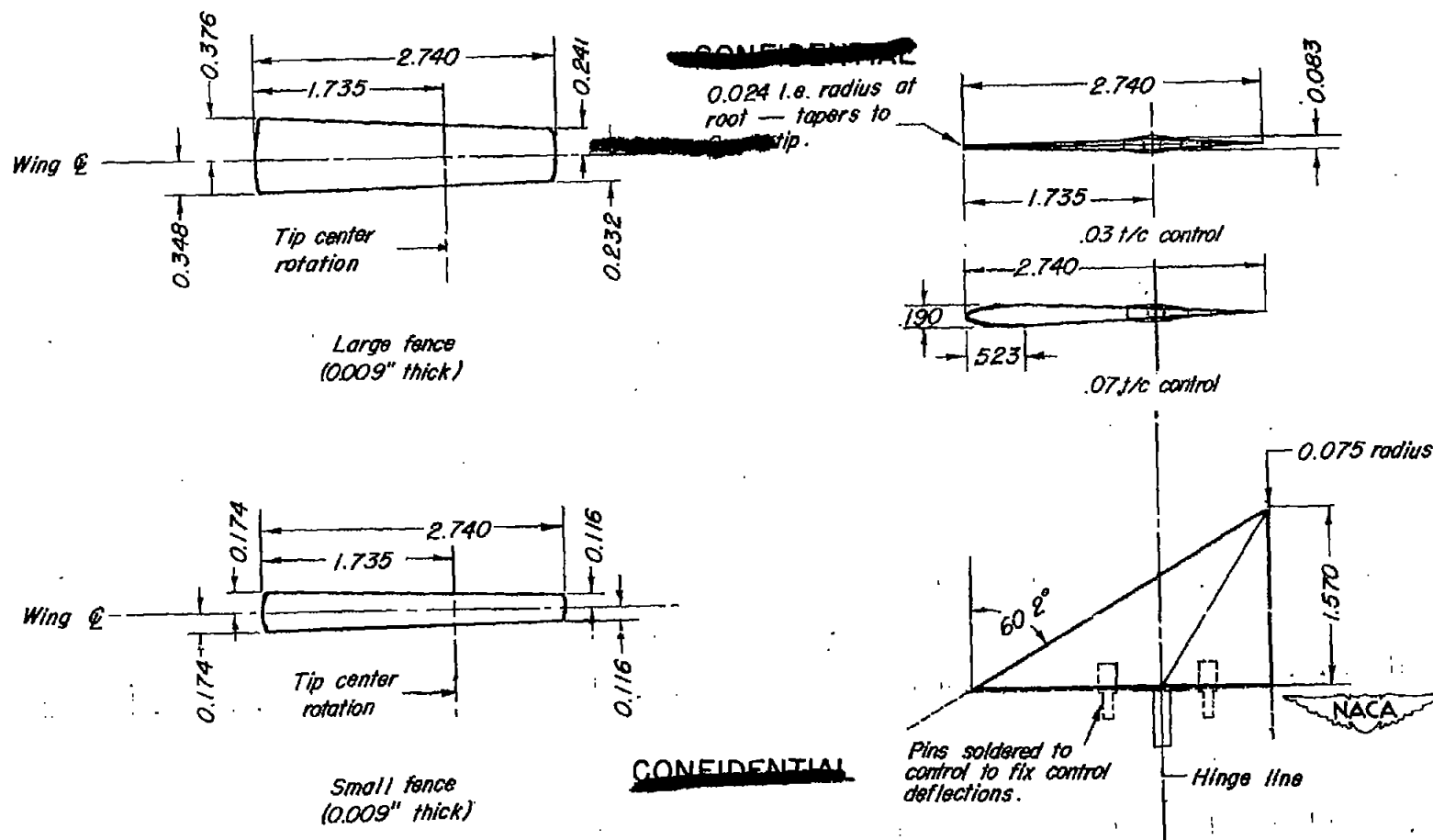
(b) Fences.

(c) Control surface; mean aerodynamic
chord, 1.83; span, 1.57.

Figure 3.- Concluded.
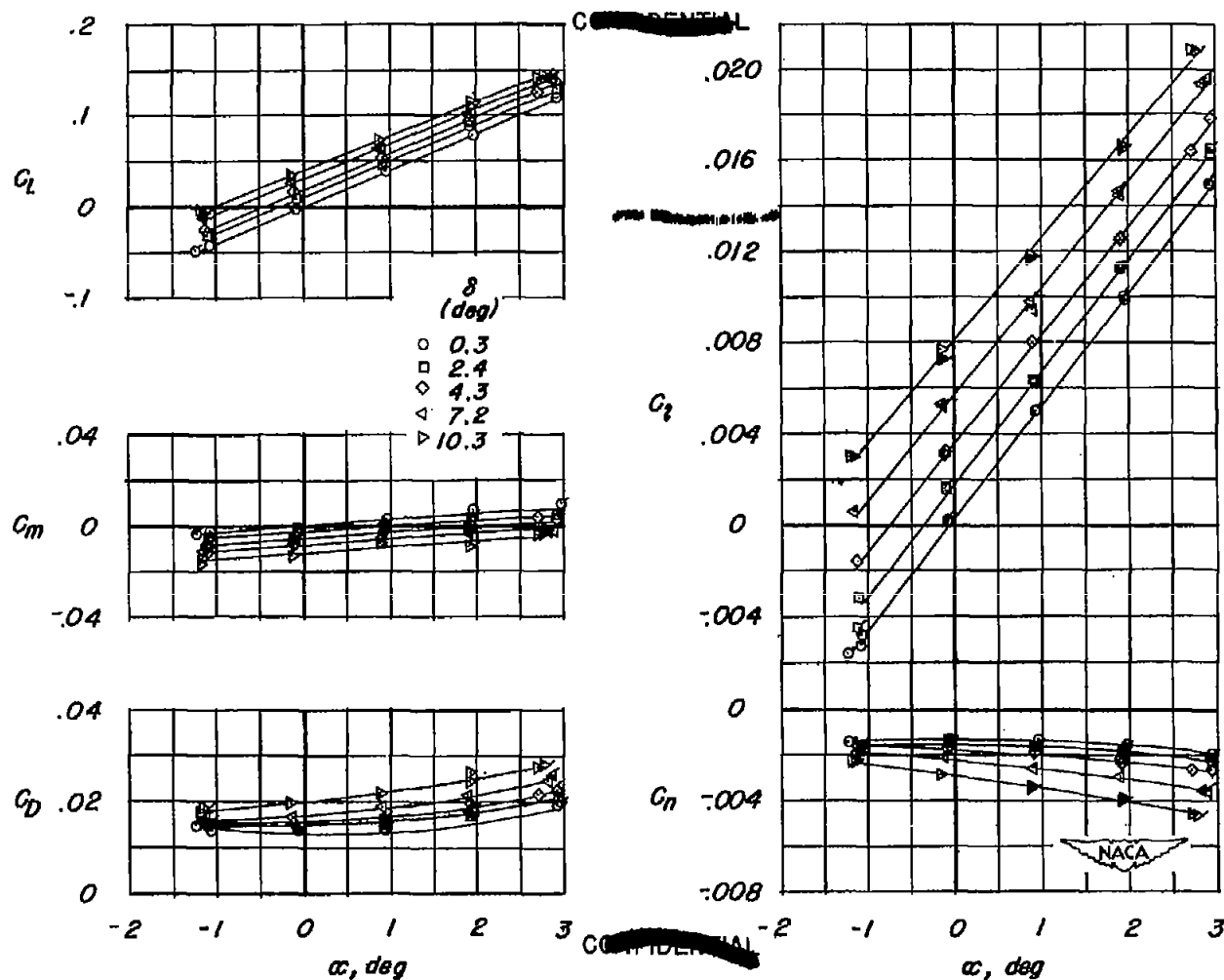
Figure 4.- Aerodynamic characteristics of a semispan delta wing with a half-delta tip control surface tested in the presence of a small fuselage. Fence off. Three-percent-thick control; R = 4.0 × 10⁶; M = 1.90. Flagged symbols denote repeat tests.
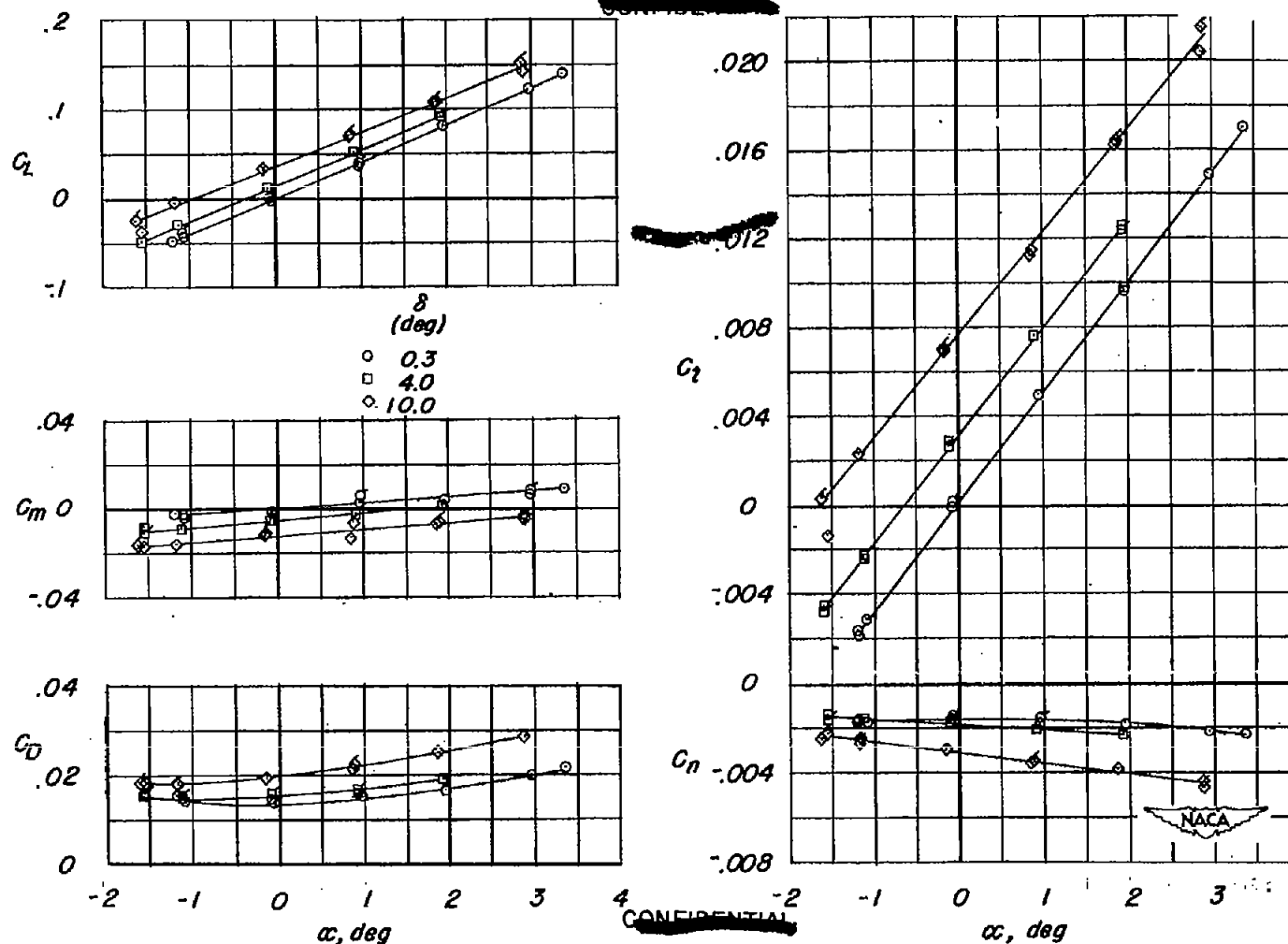
Figure 5.- Aerodynamic characteristics of a semispan delta wing with a half-delta tip control surface tested in the presence of a small fuselage. Small fence on. Three-percent-thick control; $R = 4.0 \times 10^6$; $M = 1.90$. Flagged symbols denote repeat tests.
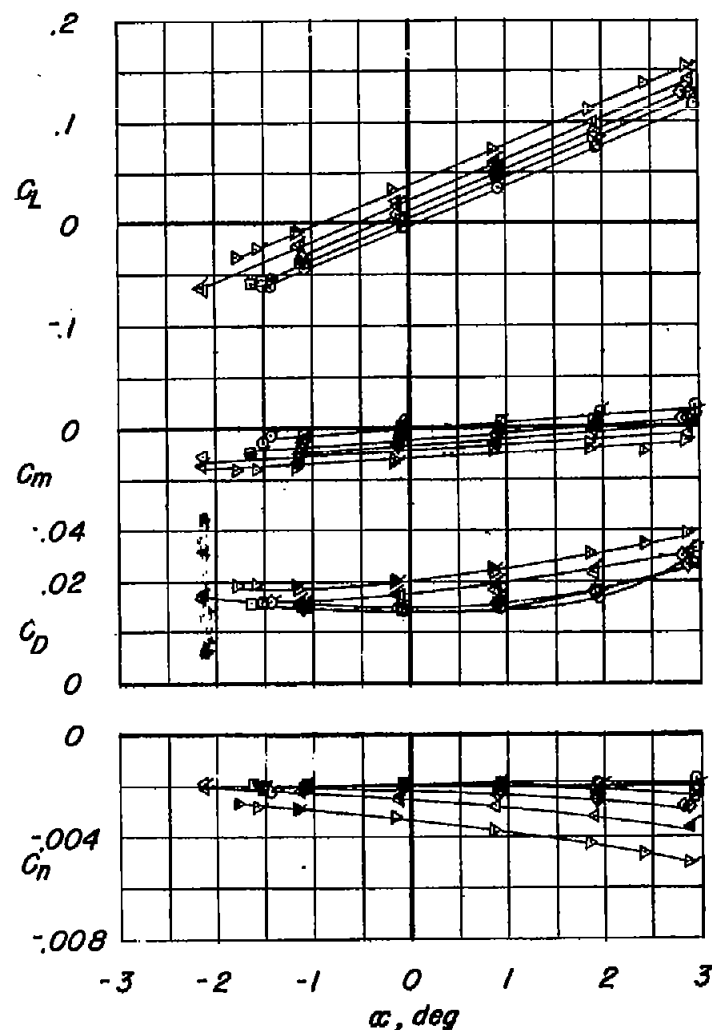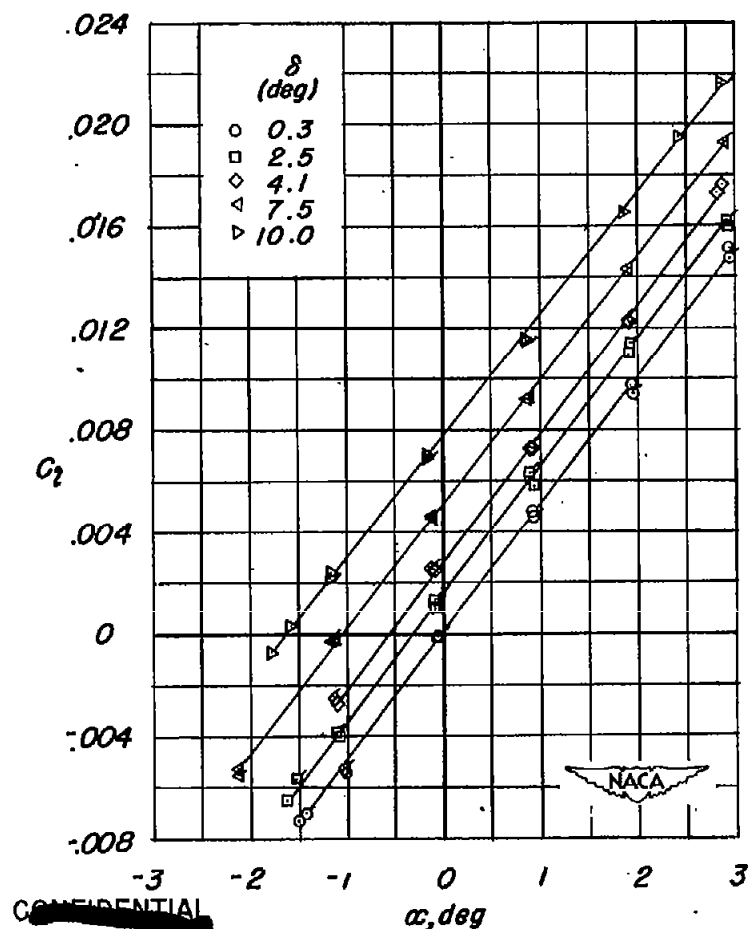
Figure 6.- Aerodynamic characteristics of a semispan delta wing with a half-delta tip control surface tested in the presence of a small fuselage. Large fence on. Three-percent-thick control; $R = 4.0 \times 10^{6}$; $M = 1.90$. Flagged symbols denote repeat tests.
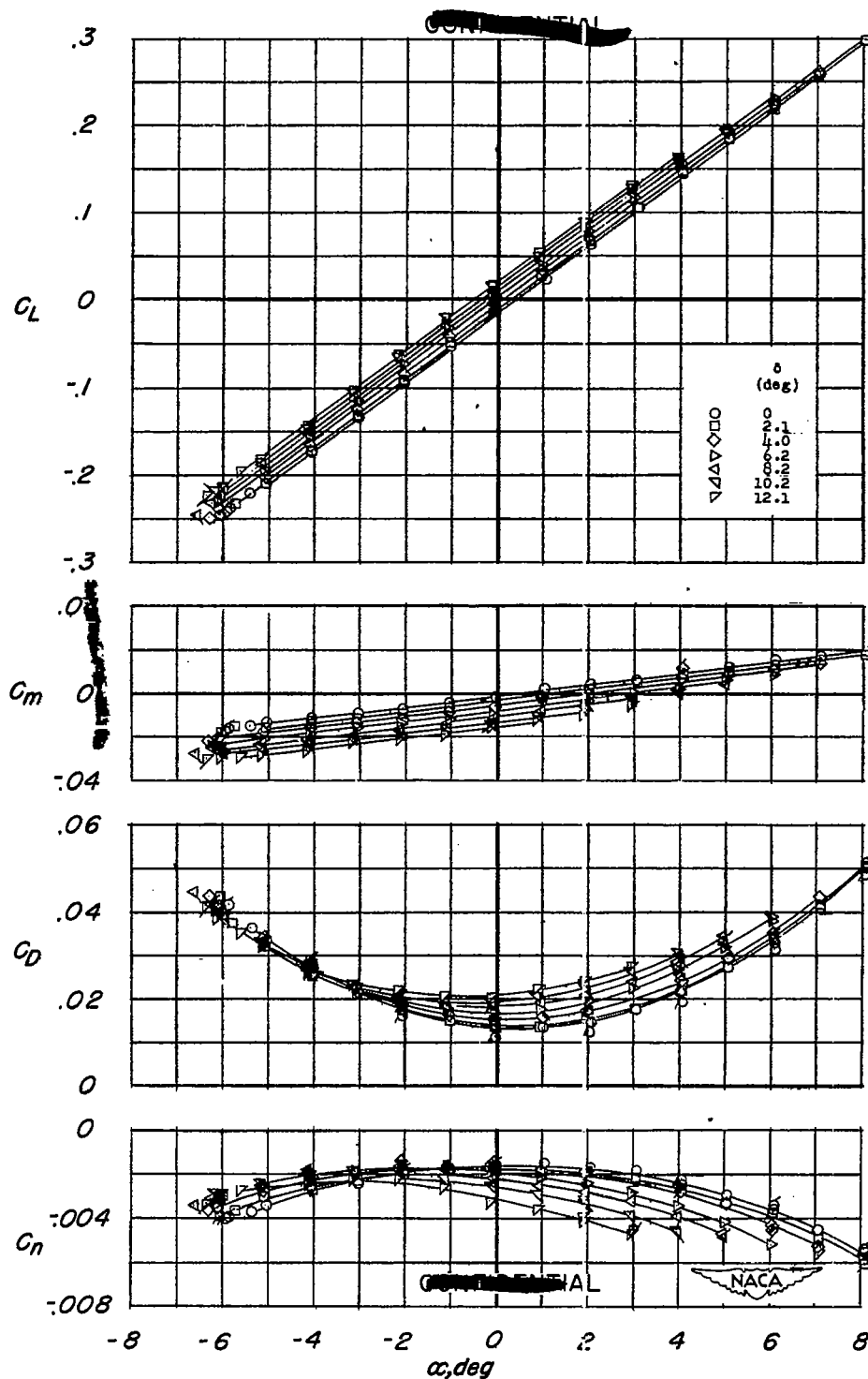
Figure 7.- Aerodynamic characteristics of a semispan delta wing with half-delta tip control surface tested in the presence of a small fuselage. Fence off. Seven-percent-thick control; R = 4.0 ⋏ 10[6]; M = 1.90. Flagged symbols denote repeat runs.
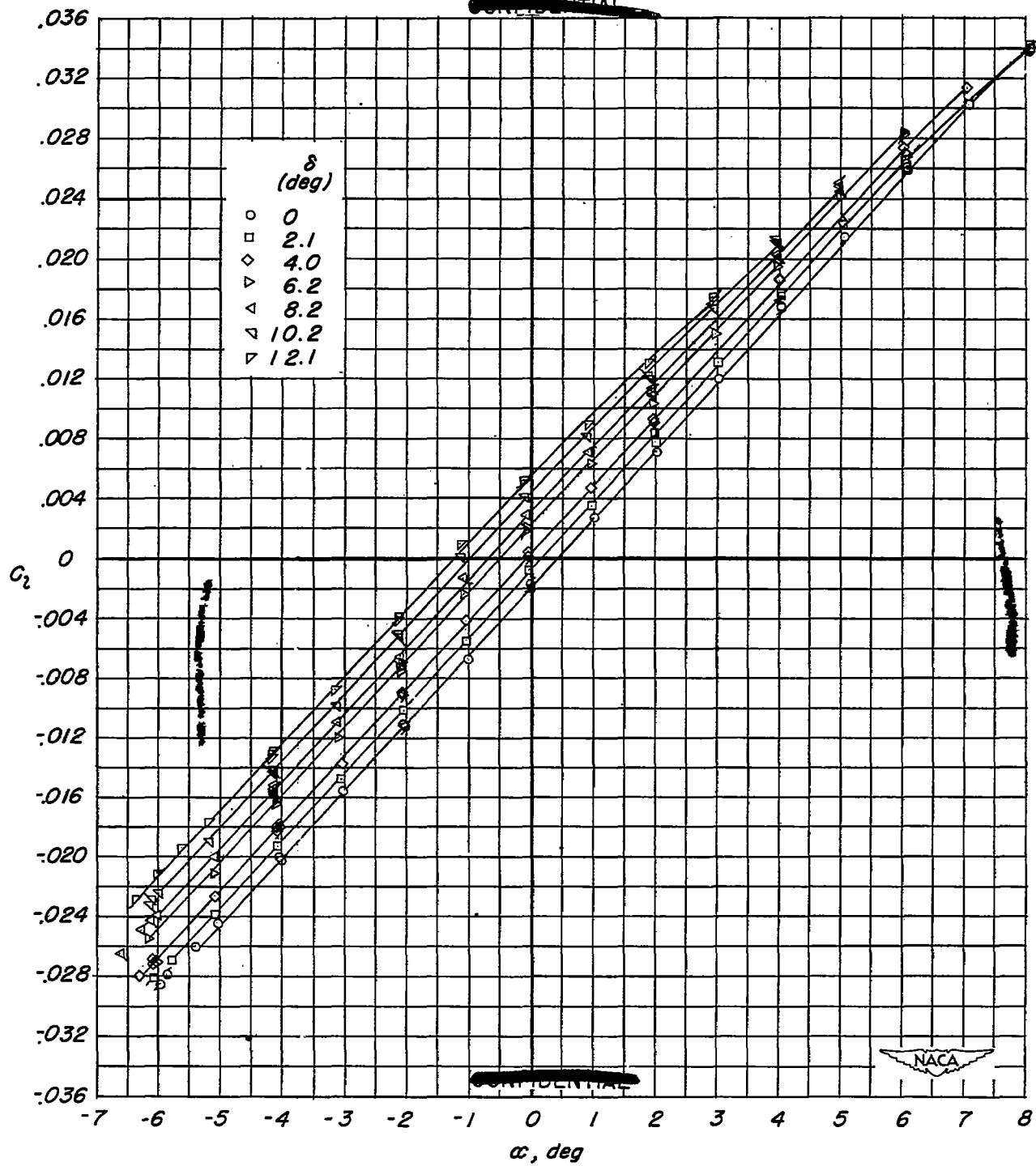
(b) Variation of C_l with α.

Figure 7.- Concluded.
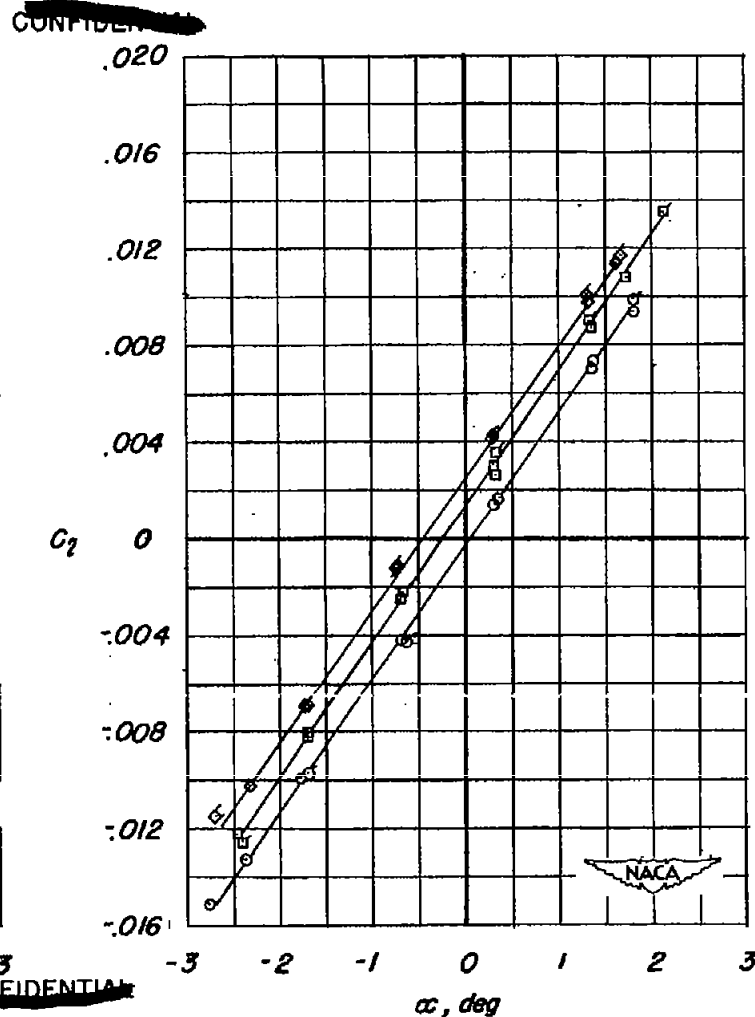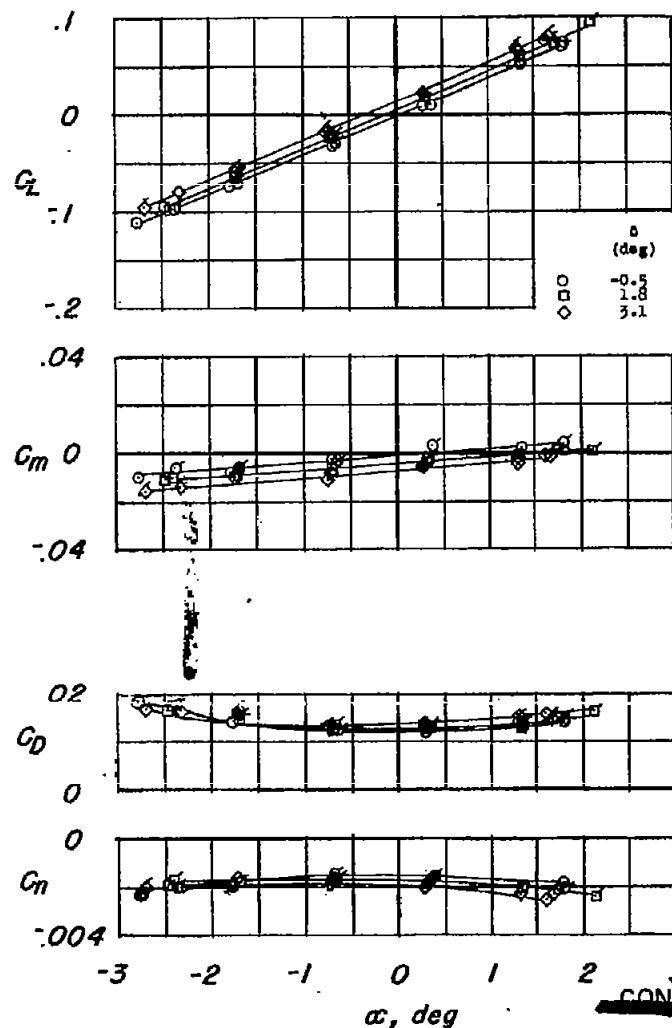
Figure 8.- Aerodynamic characteristics of a semispan delta wing with a half-delta tip control surface tested in the presence of a large fuselage. Large fence on. Three-percent-thick control; $R = 4.0 \times 10^6$; $M = 1.90$. Flagged symbols denote repeat tests.
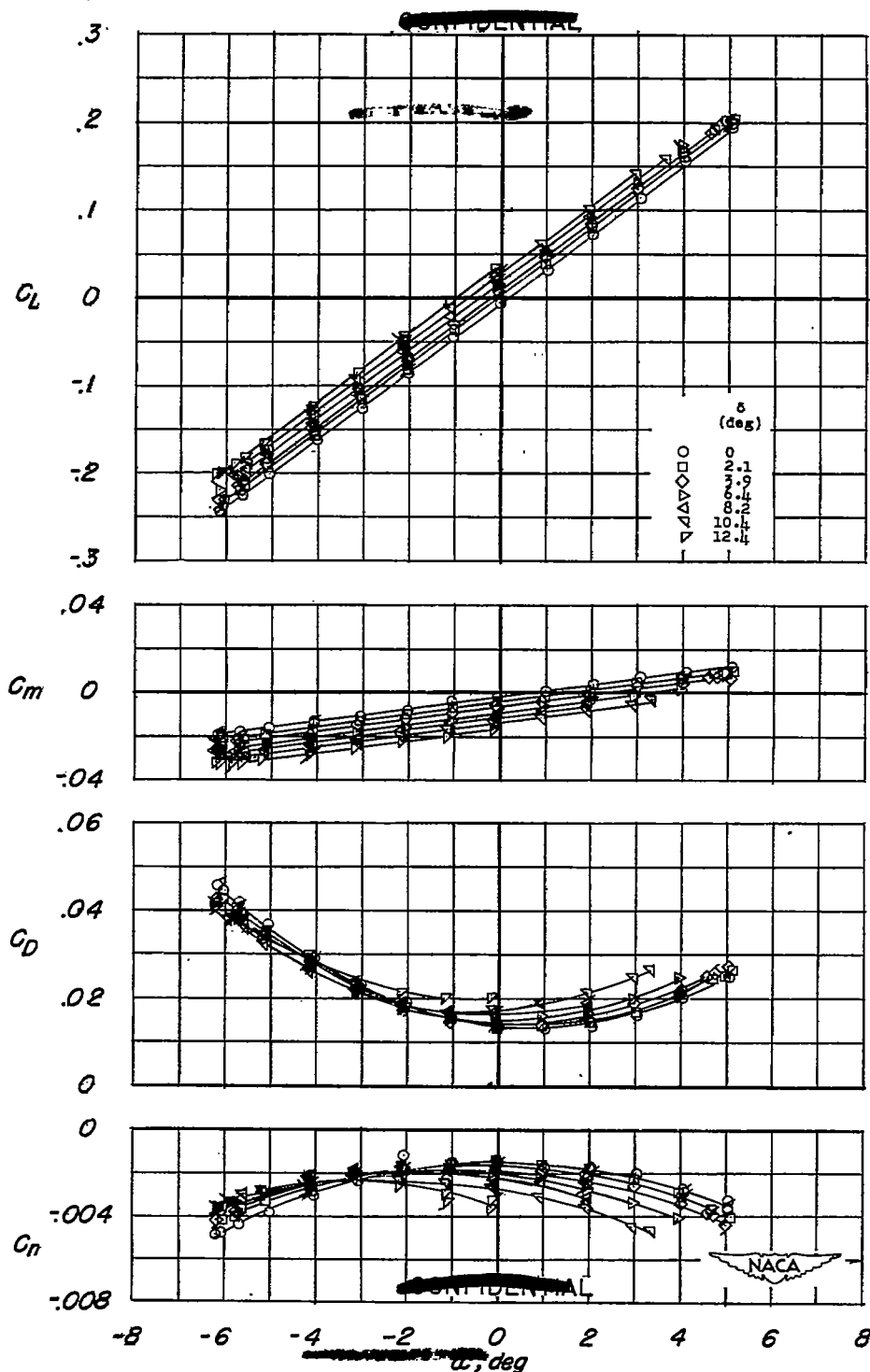
(a) Variation of C_L, C_m, C_D, and C_n with α.

Figure 9.- Aerodynamic characteristics of a semispan delta wing with a
half-delta tip control surface tested in the presence of a large
fuselage. Fence off. Seven-percent-thick control; $R = 4.0 \times 10^6$;
$M = 1.90$. Flagged symbols denote repeat tests.
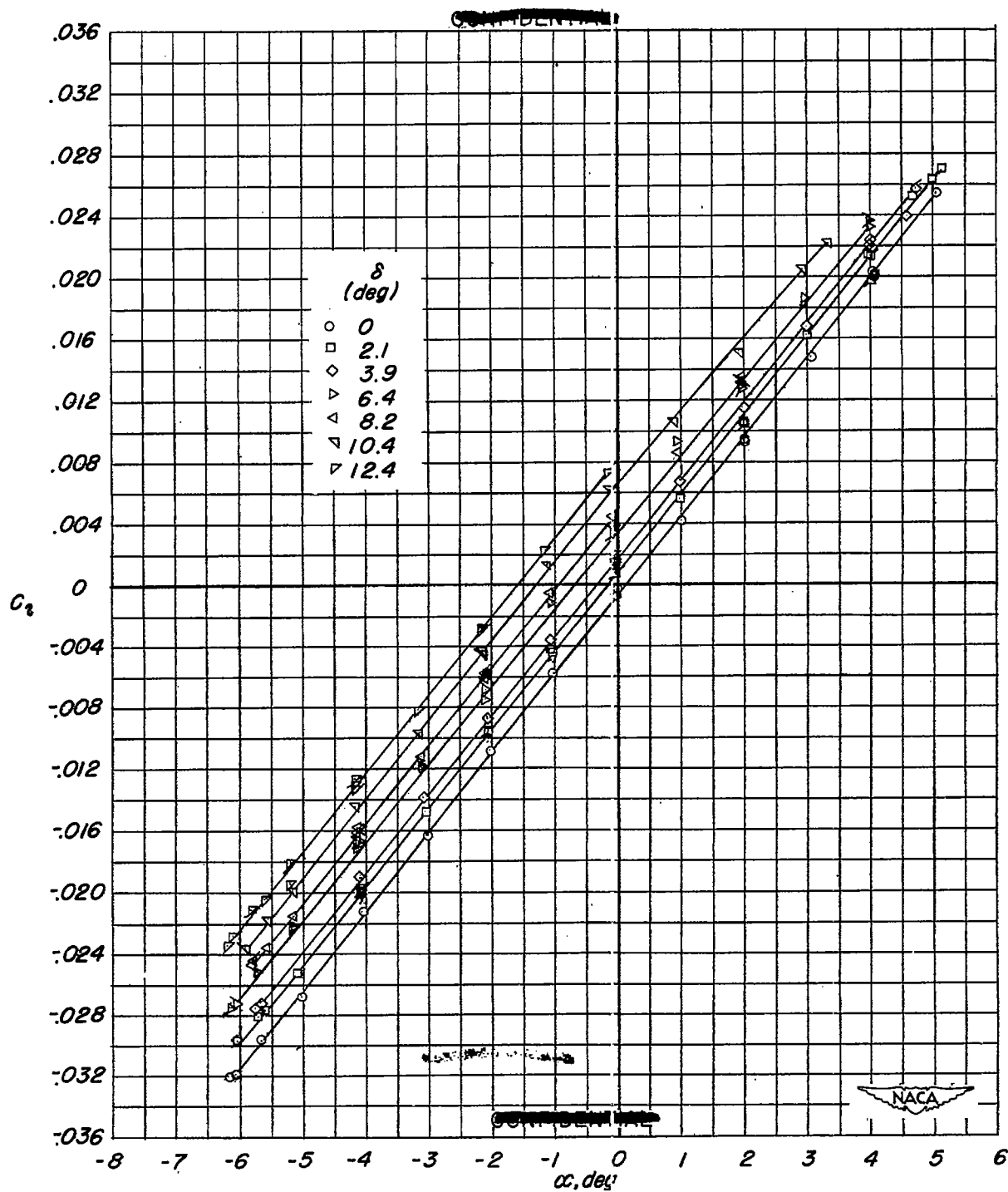
(b) Variation of C_l with α.

Figure 9.- Concluded.

(a) Small fuselage.
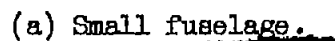
Figure 10.- Variation of the aerodynamic characteristics of a semispan delta wing with deflection of the half-delta tip control surface. $R = 4.0 \times 10^6$; $M = 1.90$; $\alpha = 0^\circ$.
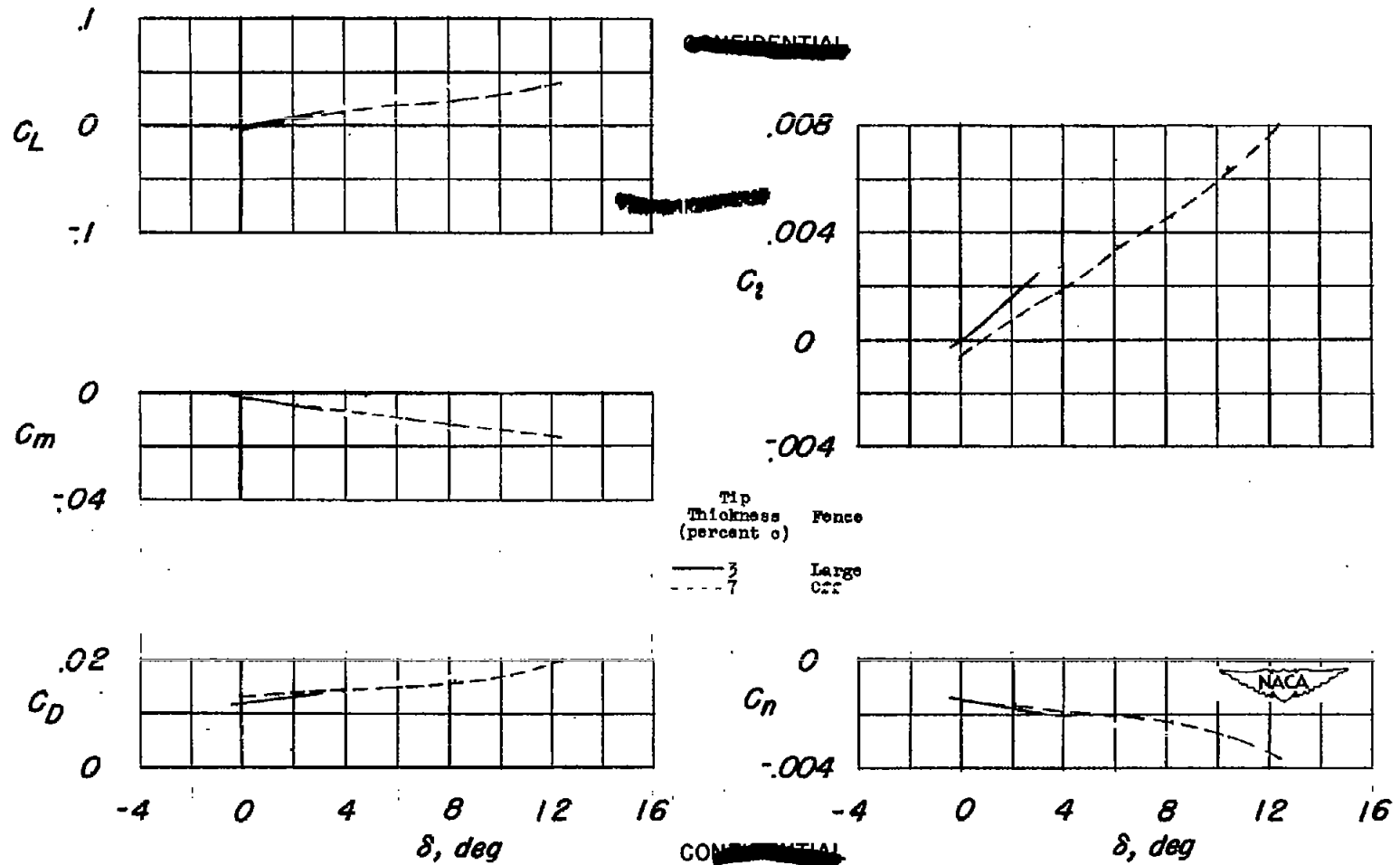
(b) Large fuselage.

Figure 10.- Concluded.

——————— Unpublished data from rocket tests
— — — — Calculation based on linearized theory

CONFIDENTIAL
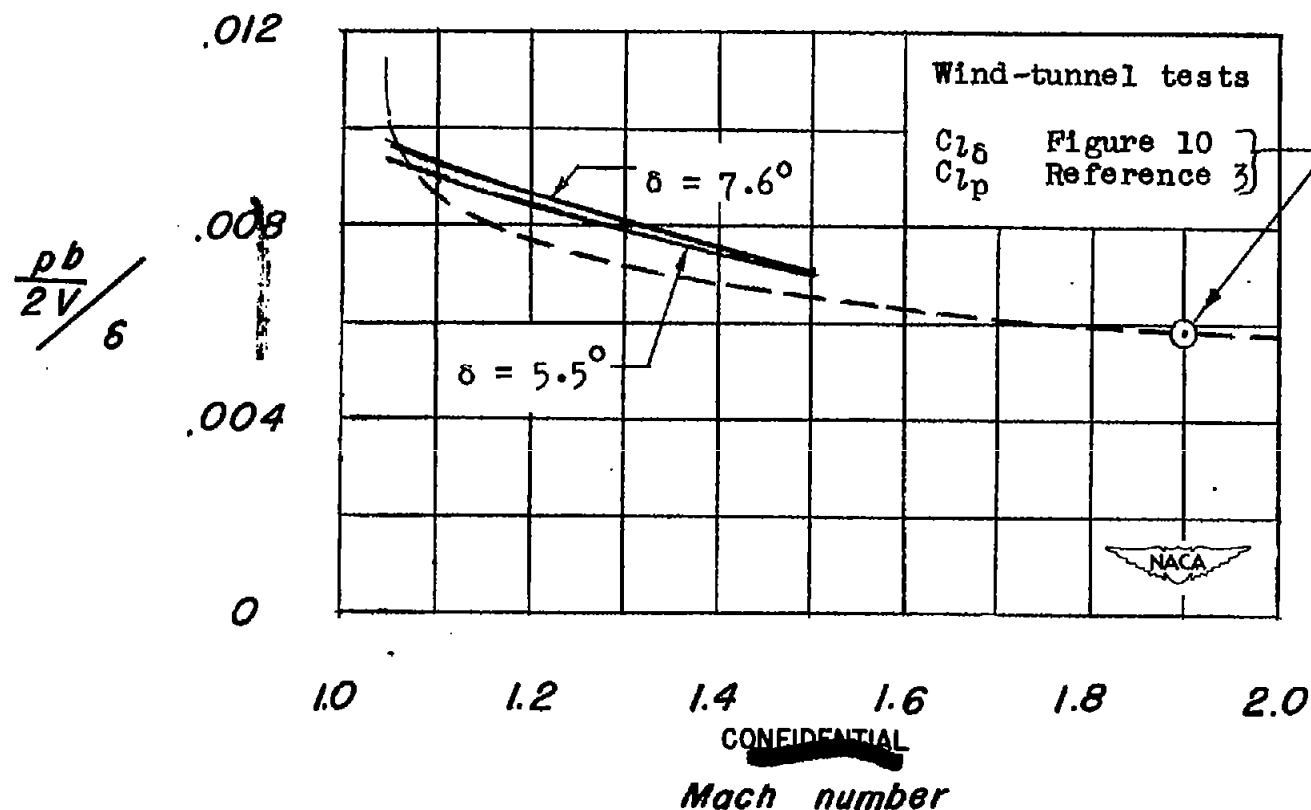
Figure 11.- Comparison of free-flight rocket test results and wind-tunnel test results with linearized theory for half-delta tip control surfaces on a delta wing-fuselage combination.
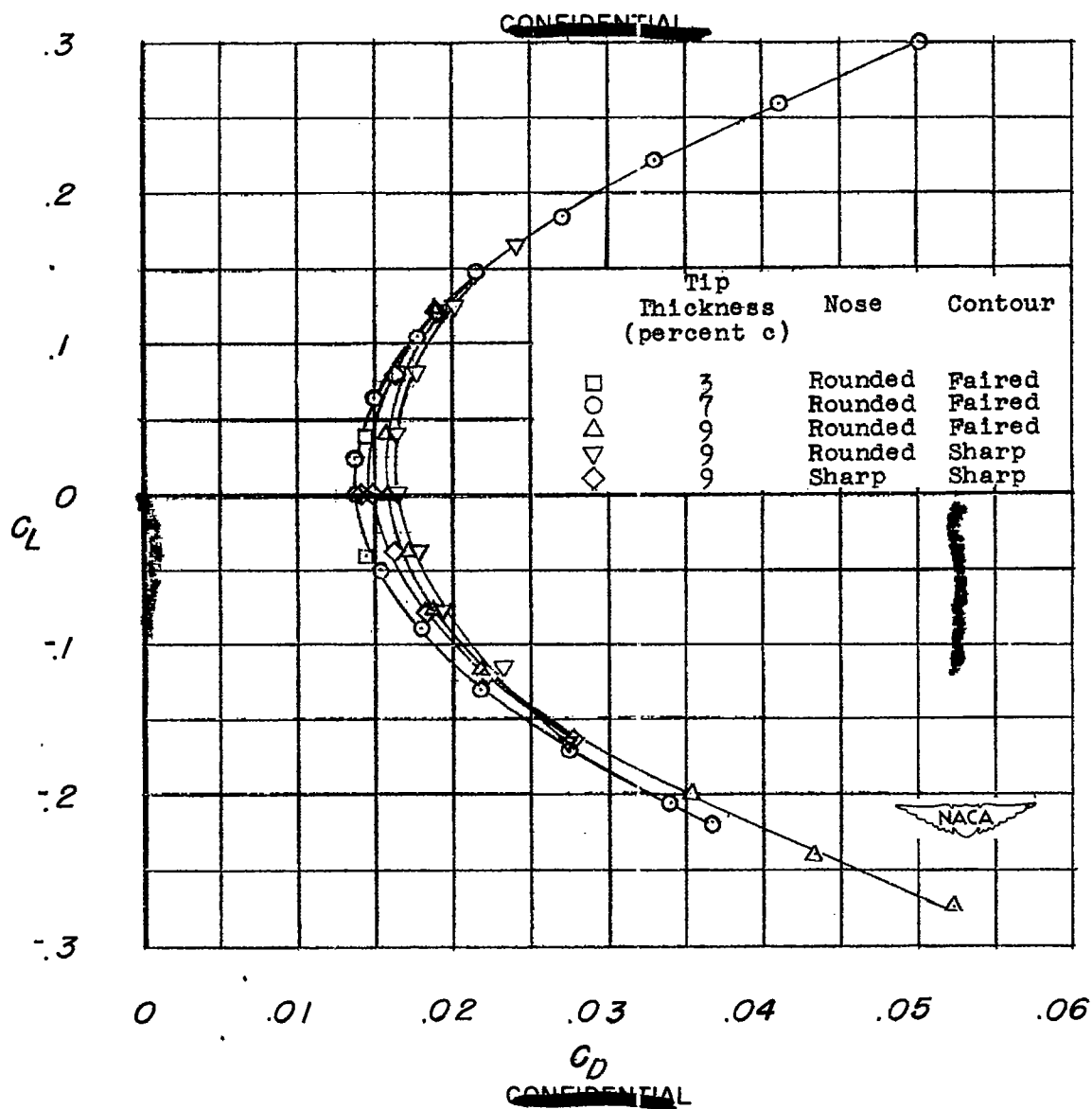
Figure 12.- Effect of tip thickness, airfoil nose radius, and airfoil contour on the lift-drag polar characteristics of a semispan delta wing. Small fuselage, fence off. R = 4.0 × 10^6; M = 1.90.

δ
(deg)

○ 0.6
□ 1.3
◇ 3.5
▷ 7.5
◁ 11.0
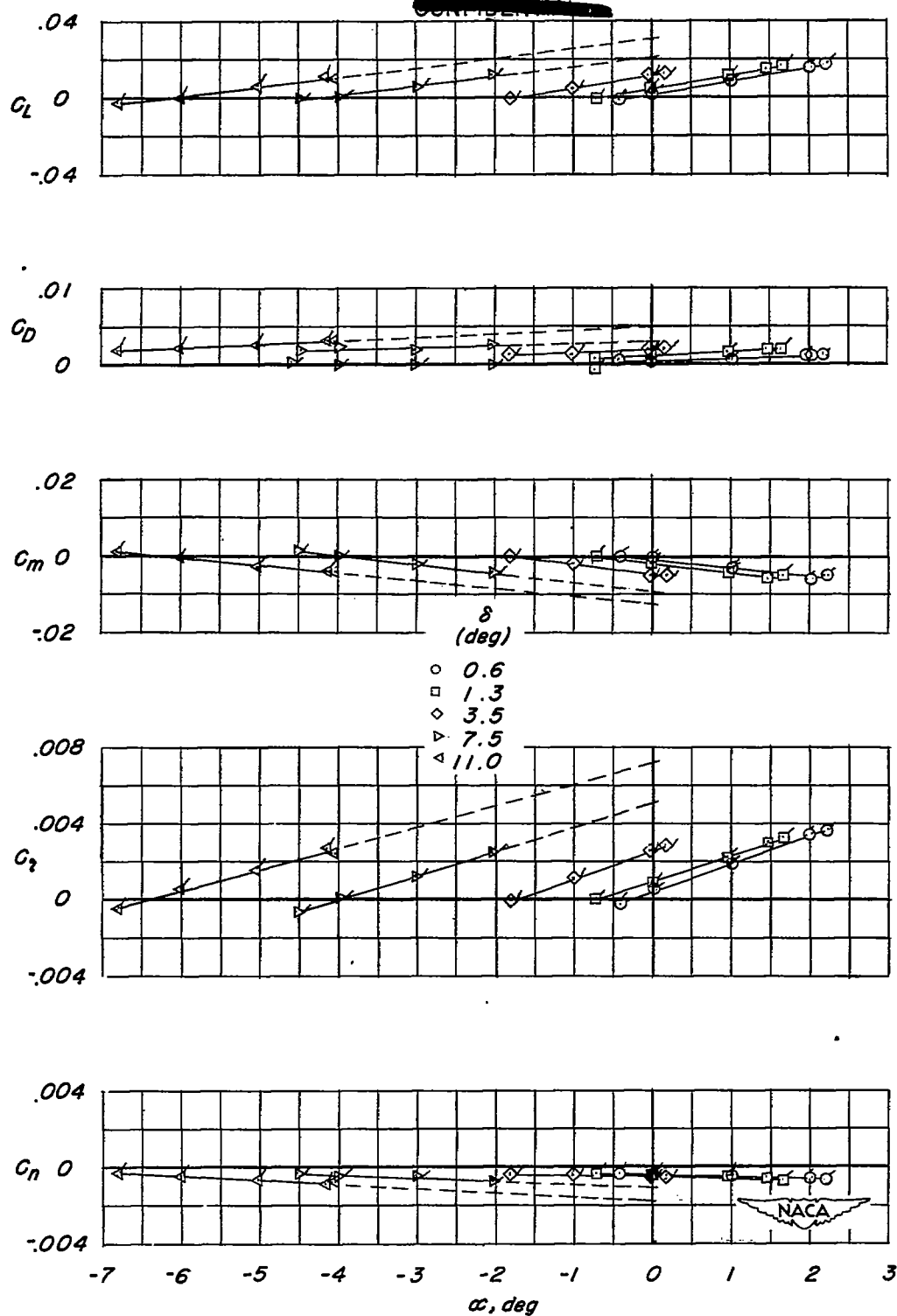
Figure 13.- Aerodynamic characteristics of a 3-percent-thick half-delta
tip control surface mounted on a semispan delta wing. Fence off.
Coefficients based on dimensions of the complete semispan wing.
M = 1.90. Flagged symbols denote repeat tests. Initial series
of tests.
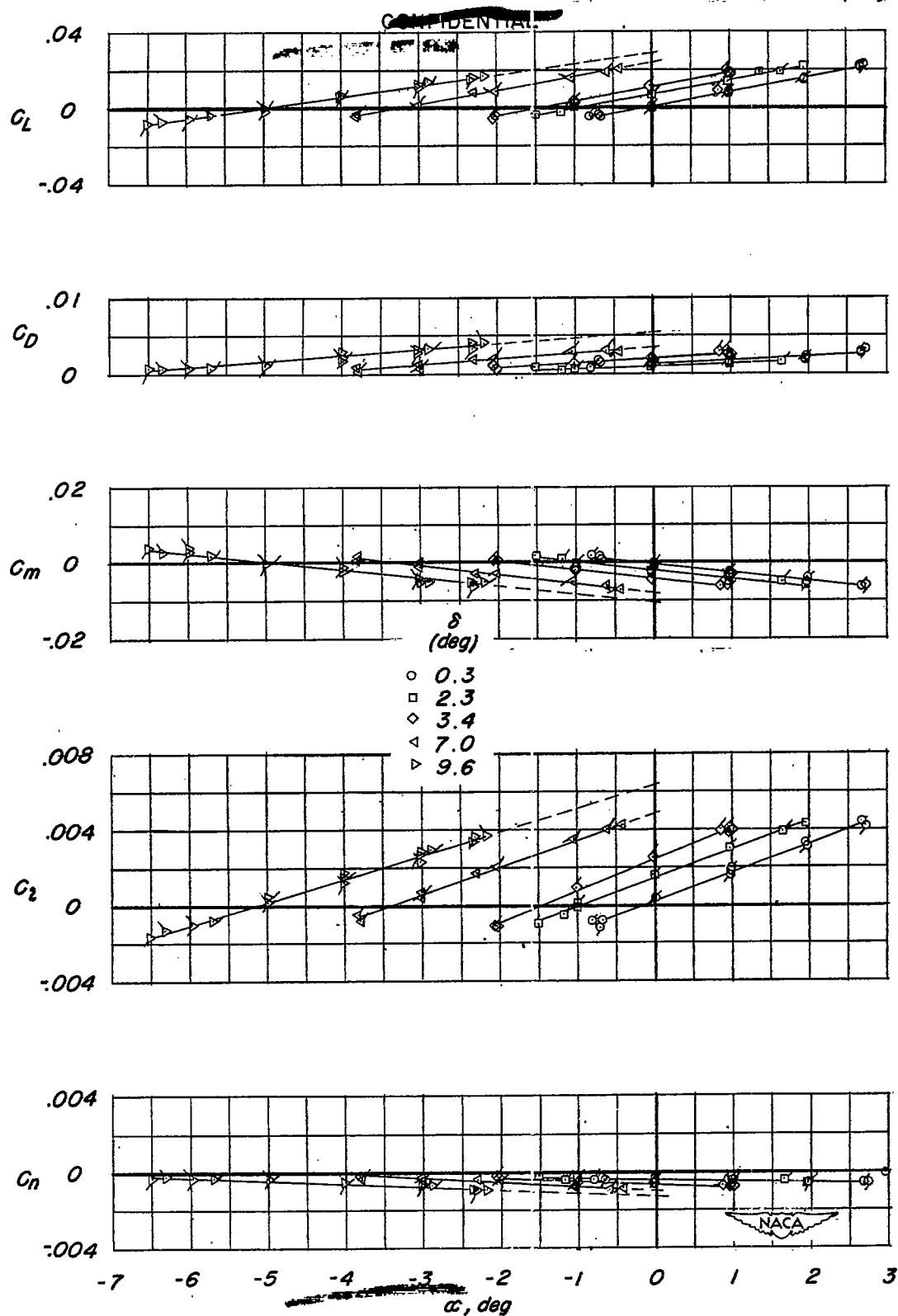
Figure 14.- Aerodynamic characteristics of a 3-percent-thick half-delta tip control surface mounted on a semispan delta wing. Large fence on. Coefficients based on dimensions of the complete semispan wing. M = 1.90. Flagged symbols denote repeat tests. Initial series of tests.
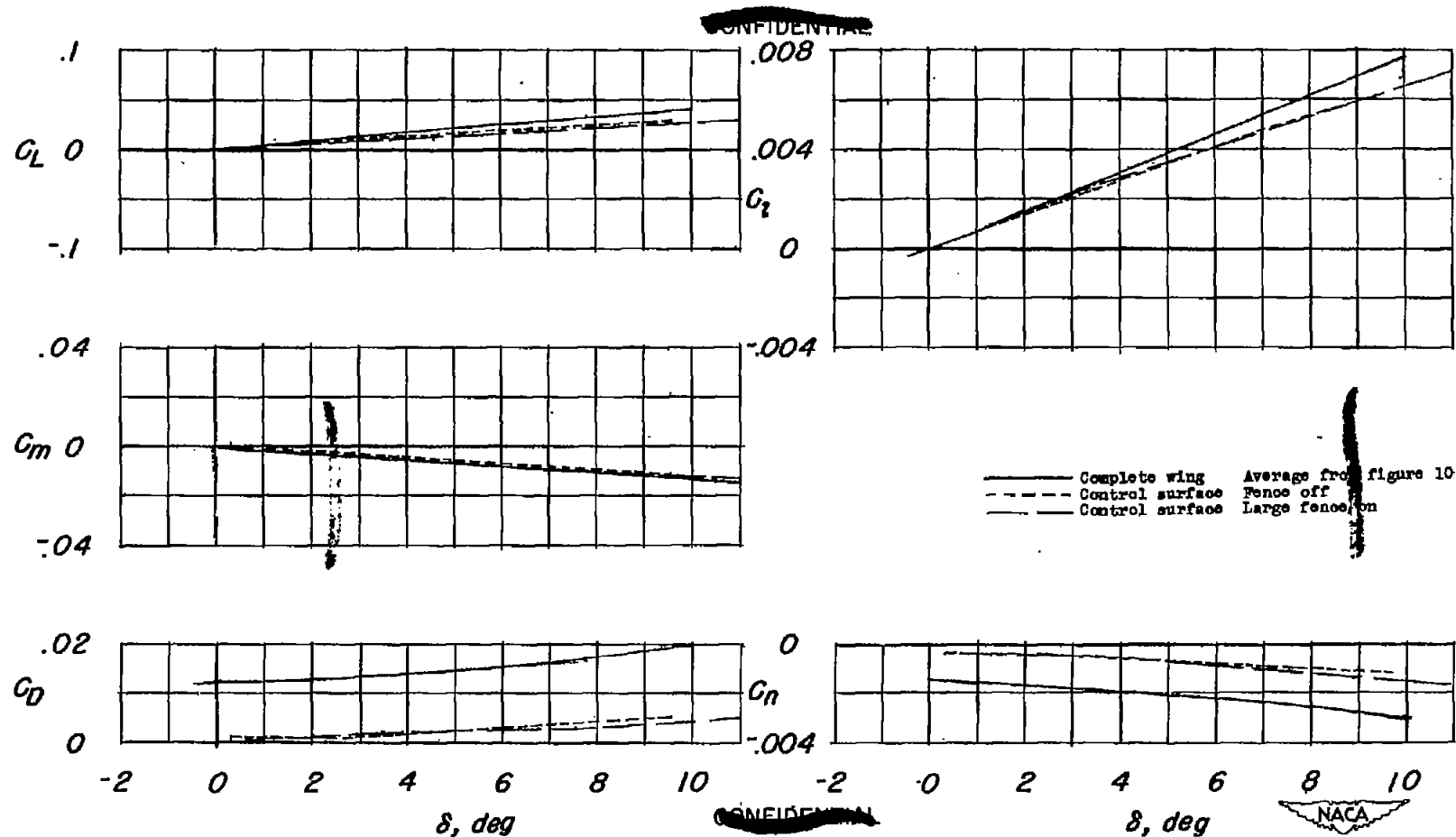
Figure 15.- Comparison between aerodynamic characteristics of the half-delta tip control surface and of the complete wing. Large fuselage, 3-percent-thick control. Variation with δ at $\alpha = 0°$; $R = 4.0 \times 10^6$; $M = 1.90$.
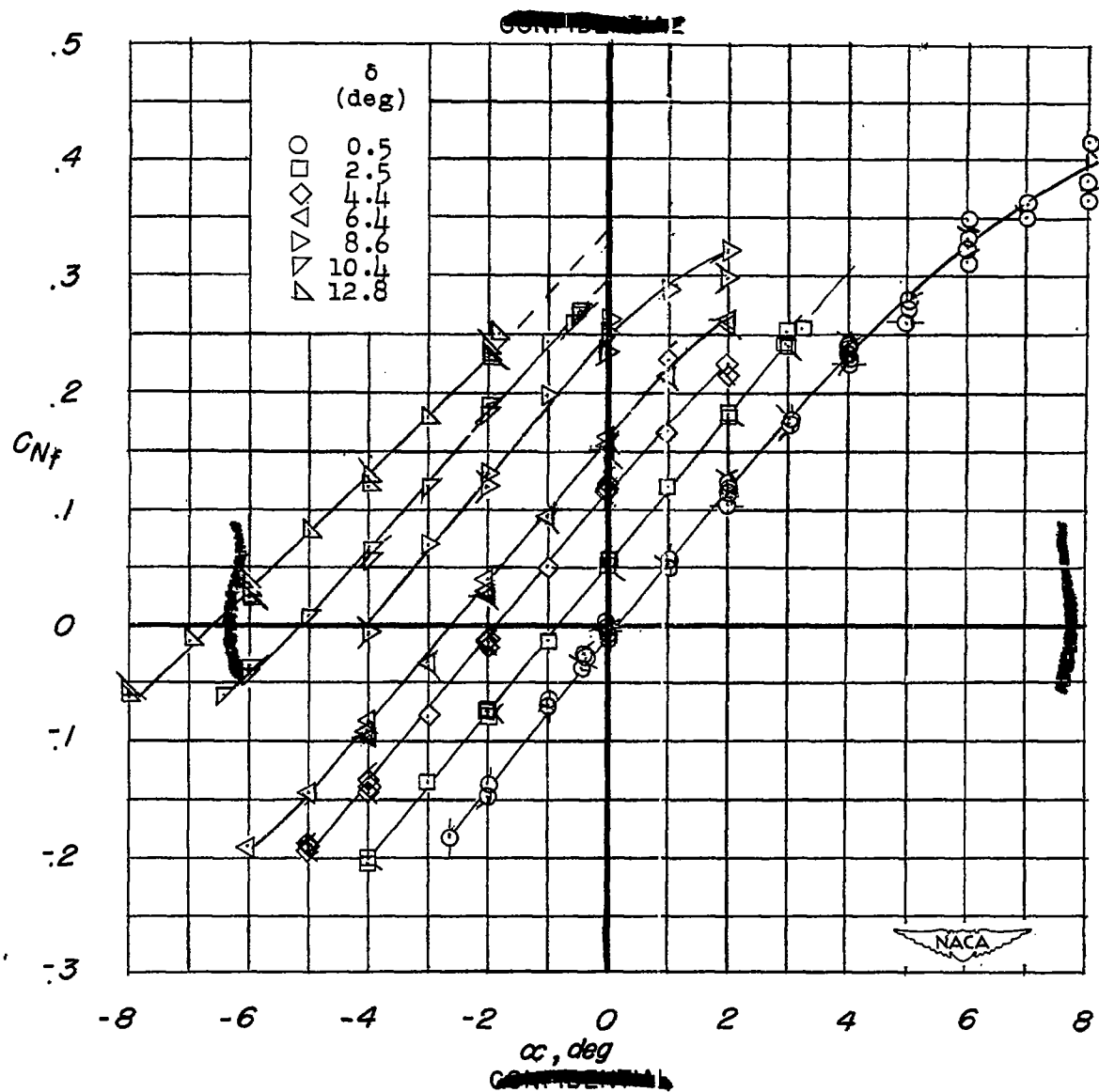
(a) Normal force plotted against α.

Figure 16.- Aerodynamic loading characteristics of a 0.03t/c half-delta
control surface. Fence off. Data presented with respect to control
surface axes. R = 4.0 × 10⁶; M = 1.90. Second series of tests.
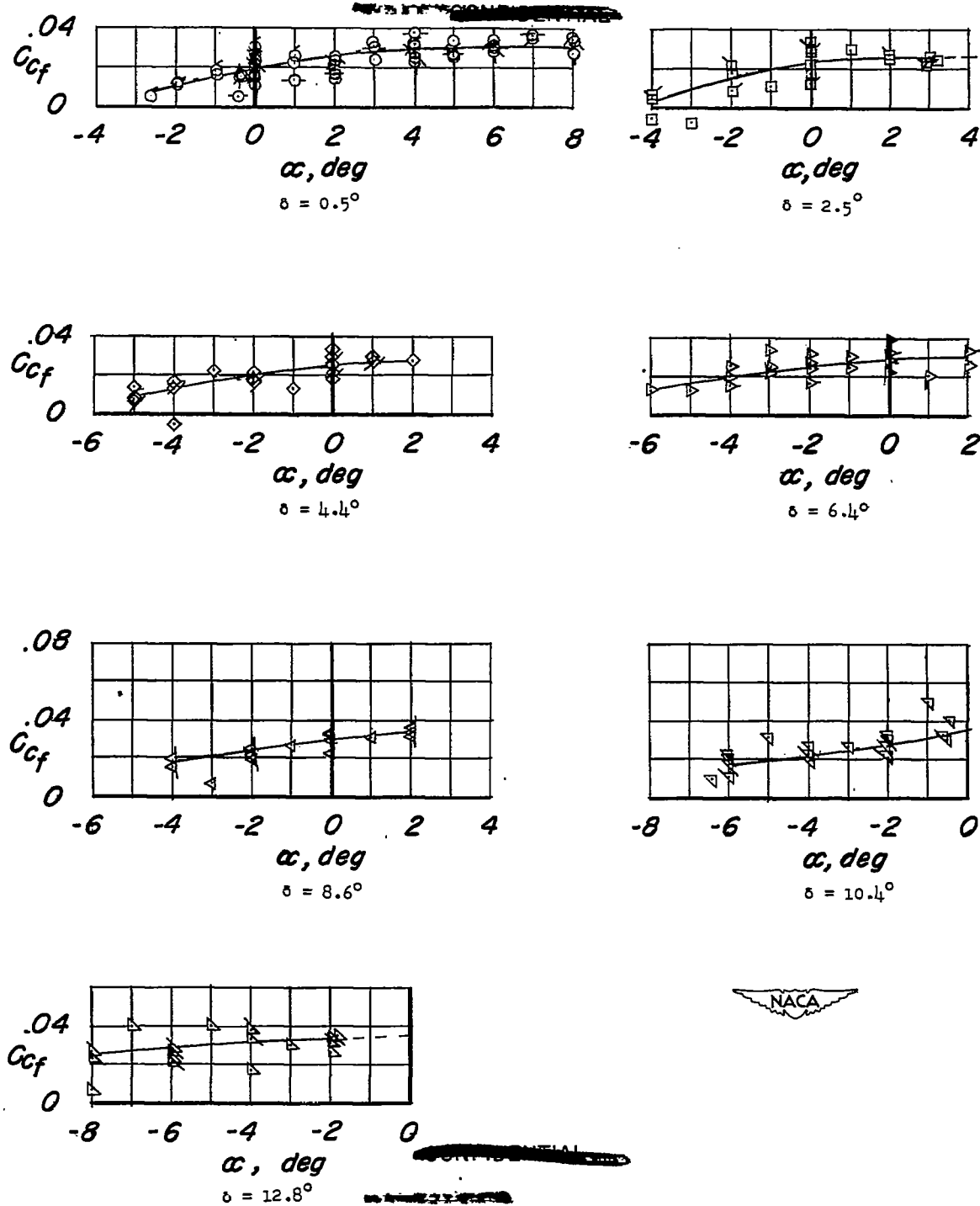
(b) Chord force plotted against α.

Figure 16.- Continued.
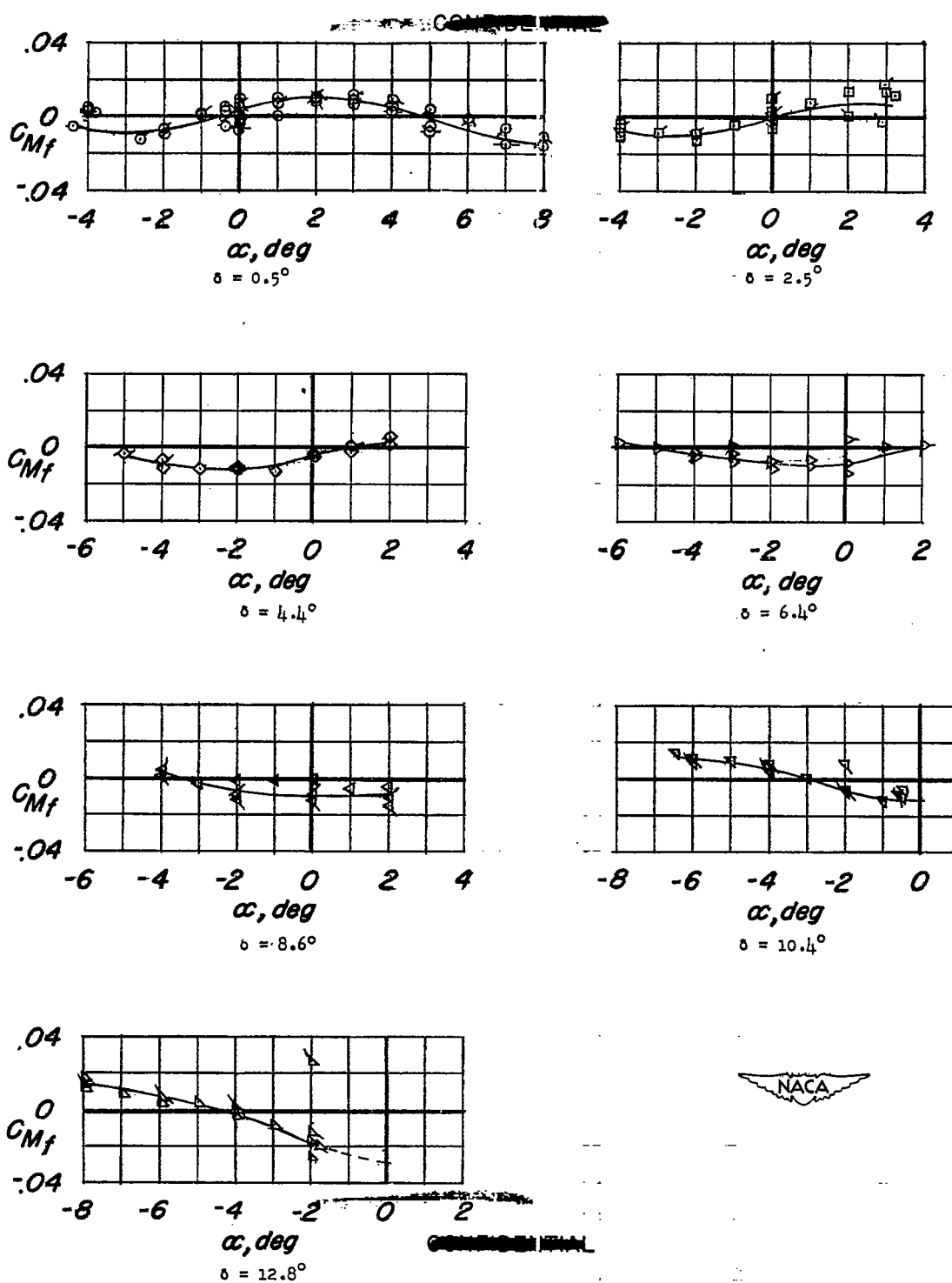
(c) Hinge moment plotted against α.

Figure 16.- Continued.
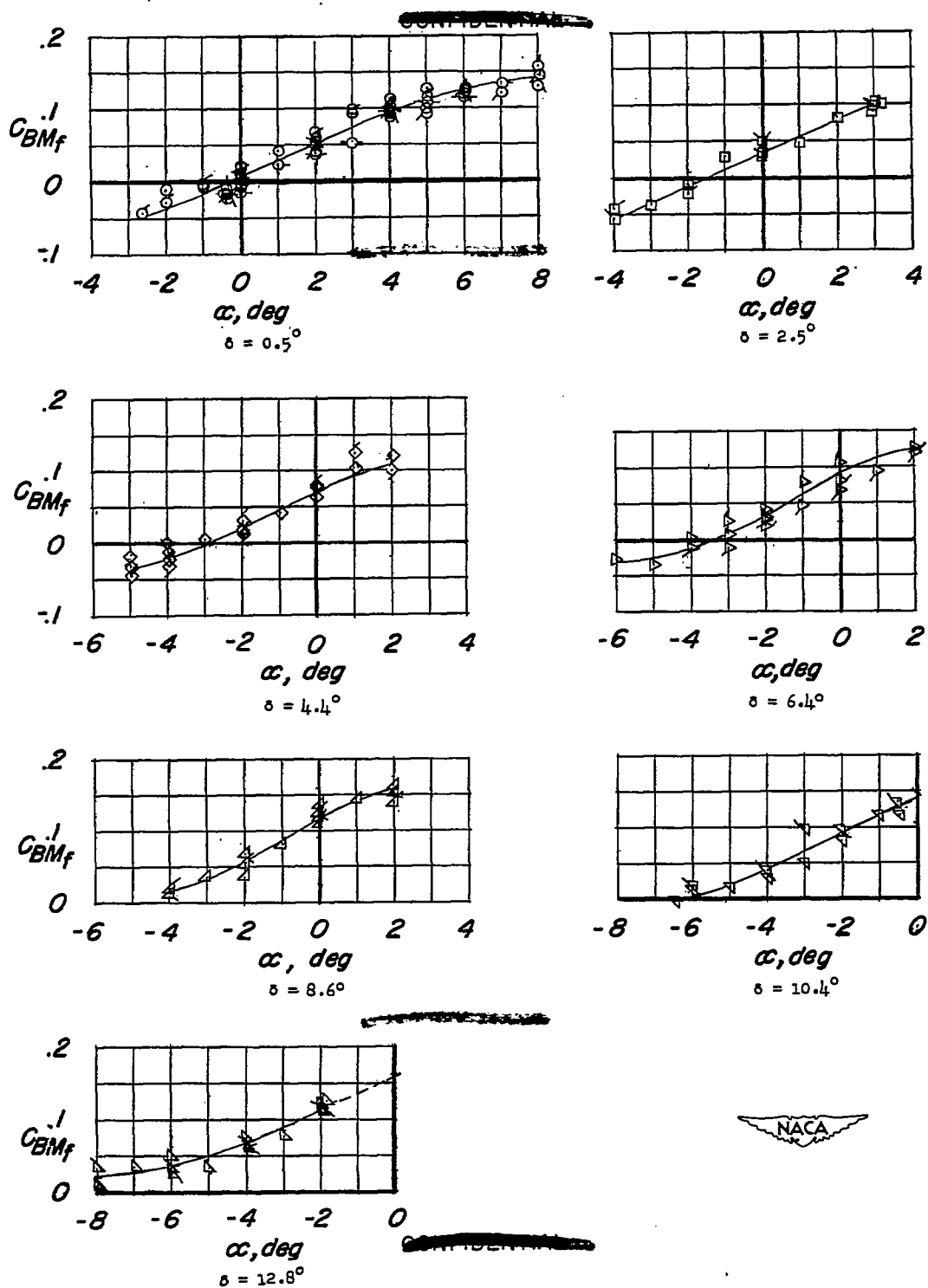
(d) Bending moment plotted against α.

Figure 16.- Concluded.
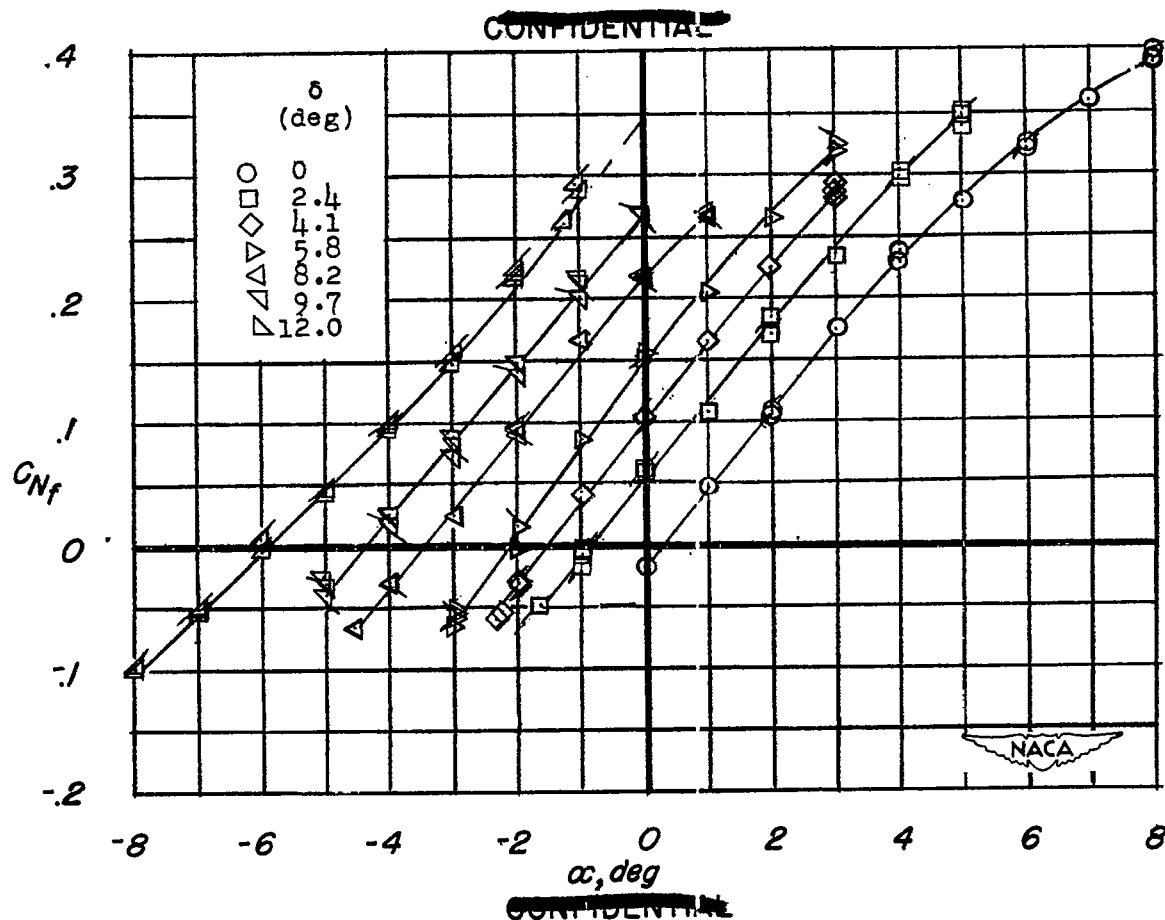
(a) Normal force plotted against α.

Figure 17.- Aerodynamic loading characteristics of a 0.07t/c half-delta
control surface. Fence off. Data presented with respect to control
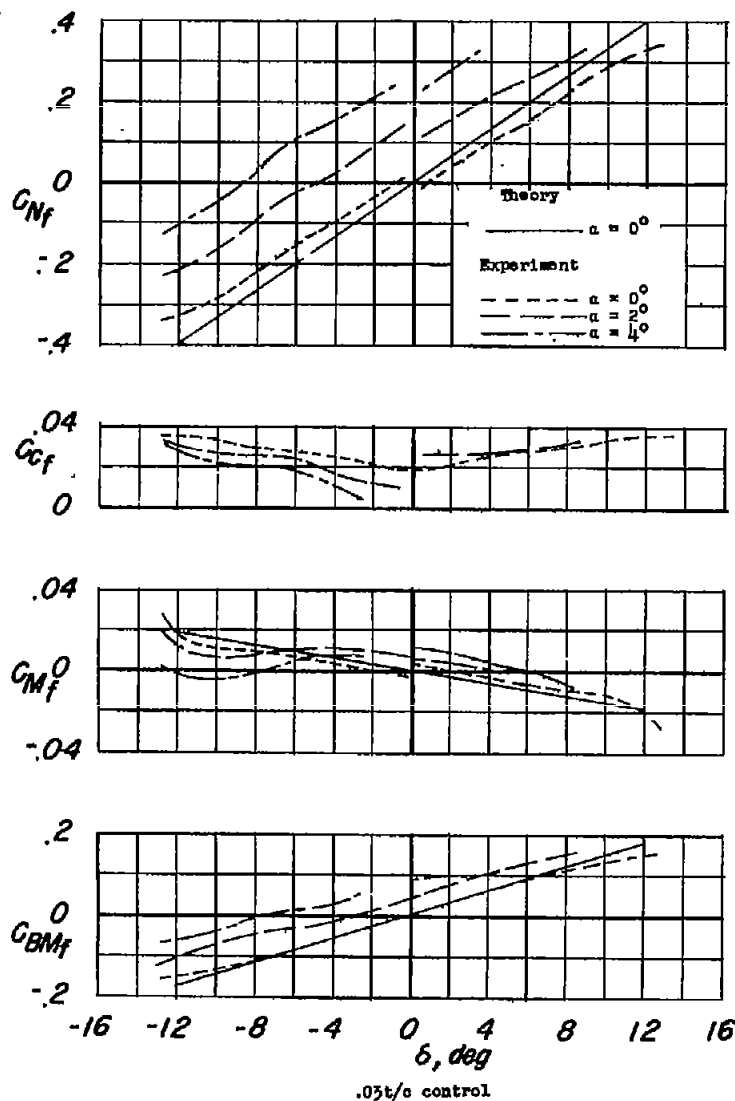surface axes. Second series of tests.
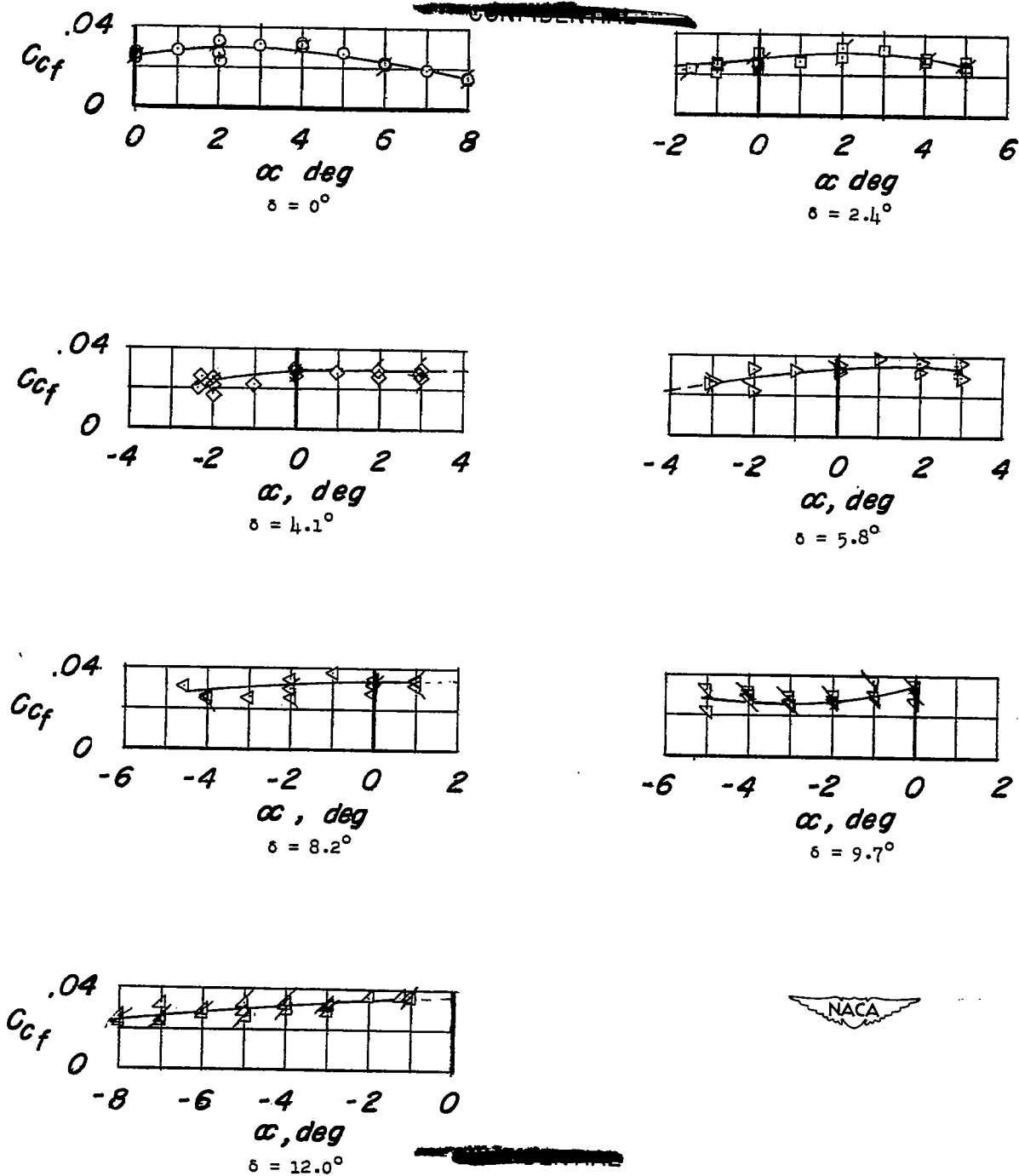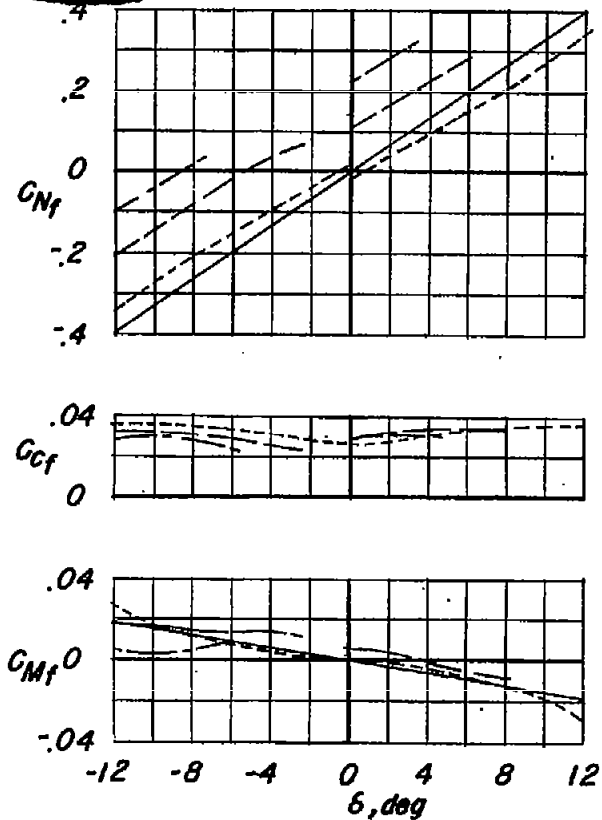
(b) Chord force plotted against α.

Figure 17.- Continued.
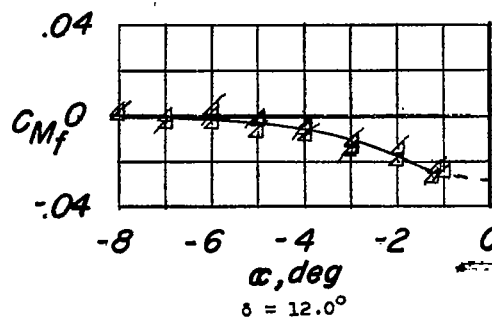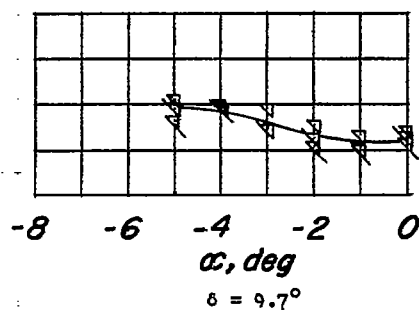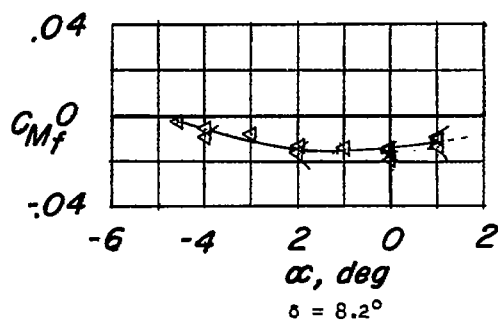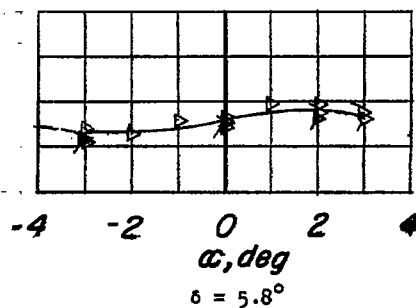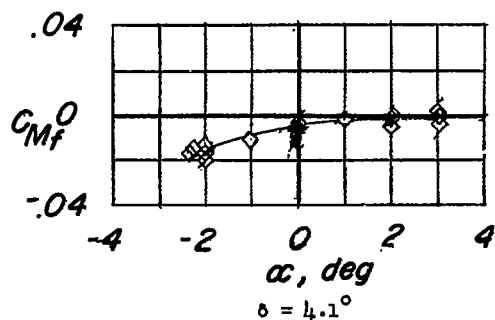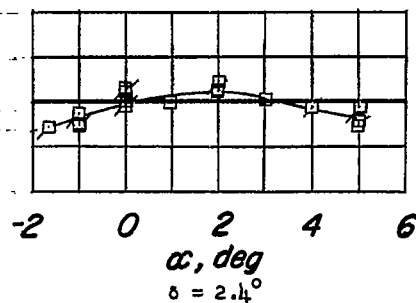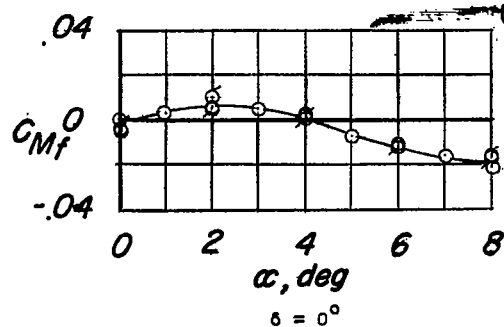
(c) Hinge moment plotted against α.

Figure 17.- Concluded.

Figure 18.- Variation of the aerodynamic characteristics with deflection of two half-delta control surfaces tested in presence of a semispan delta wing.